Available online at www.sciencedirect.com

ScienceDirect

Geochimica et Cosmochimica Acta 172 (2016) 177–204

Geochimica et Cosmochimica Acta

www.elsevier.com/locate/gca

Biological source and provenance of deep-water derived isoprenoid tetraether lipids along the Portuguese continental margin

Jung-Hyun Kim [a,*,1,2], Laura Villanueva [a,2], Claudia Zell [a], Jaap S. Sinninghe Damsté [a,b]

[a] *NIOZ Royal Netherlands Institute for Sea Research, Department of Marine Organic Biogeochemistry, NL-1790 AB Den Burg, The Netherlands*

[b] *Utrecht University, Faculty of Geosciences, P.O. Box 80.021, 3508 TA Utrecht, The Netherlands*

Received 8 February 2015; accepted in revised form 3 September 2015; available online 22 October 2015

Abstract

There is increasing evidence that nitrifying Thaumarchaeota in the deep ocean waters may contribute to the sedimentary composition of isoprenoid glycerol dialkyl glycerol tetraethers (isoGDGTs), impacting TEX_{86} paleothermometry. We investigated the potential effect of deep-water dwelling Thaumarchaeota in the warm and saline Mediterranean Outflow Water (MOW) on the distribution of isoGDGTs by analysing suspended particulate matter (SPM) and surface sediments collected along five land-ocean transects along the southern Portuguese continental margin. To this end, we directly compared for the first time the composition of intact polar lipid (IPL)-derived isoGDGTs of SPM with the diversity, abundance, and activity of Thaumarchaeota based on the genetic analysis of the genes coding for the archaeal ammonia monooxygenase (*amo*A) and the geranylgeranylglyceryl phosphate (GGGP) synthase involved in the isoGDGT biosynthetic pathway. Our results revealed a strong positive relationship between water depth and TEX_{86}^{H} values for both SPM and surface sediments. The increasing TEX_{86}^{H} trends for both core lipid (CL) and IPL-derived fractions were accompanied by increasing fractional abundances of GDGT-2 and crenarchaeol regio-isomer and decreasing fractional abundances of GDGT-1 and GDGT-3 with increasing water depth. Phylogenetic analyses based on the archaeal *amo*A and the GGGP synthase proteins showed that Thaumarchaeota populations detected at 1 m and 50 m water depth were different from those detected in 200 m and 1000 m water depth, which had an increased contribution of so-called 'deep water' Thaumarchaeota. The differences in the fractional abundances of isoGDGTs with water depth were compatible with the increasing contribution of 'deep water' Thaumarchaeota harboring a different GGGP synthase enzyme which has been suggested to relate to changes in the relative proportion of synthesized isoGDGTs. Accordingly, it appears that the sedimentary distribution of CL isoGDGTs used in TEX_{86}^{H} along the Portuguese margin is primarily influenced by water depth due to the increasing contribution of the deep-water population of Thaumarchaeota residing in the MOW. Our study also reveals that the effect of deep water Thaumarchaeotal communities on sedimentary isoGDGT distributions should be considered globally.

* Corresponding author. Tel.: +82 (0)10 3902 2329.
E-mail address: jhkim123@hanyang.ac.kr (J.-H. Kim).
[1] Present address: Department of Marine Science and Convergence Technology, Hanyang University ERICA Campus, 55 Hanyangdaehak-ro, Sangnok-gu, Ansan-si, Gyeonggi-do 426-791, South Korea.
[2] The authors contributed equally to this work.

http://dx.doi.org/10.1016/j.gca.2015.09.010
0016-7037/

1. INTRODUCTION

In the marine water column, Thaumarchaeota, formerly known as Marine Group I Crenarchaeota (e.g. Brochier-Armanet et al., 2008; Spang et al., 2010), are one of the dominant prokaryotes in today's oceans (e.g. Karner et al., 2001; Herndl et al., 2005). Thaumarchaeota produce isoprenoid glycerol dialkyl glycerol tetraethers (isoGDGTs) as their major membrane building blocks containing 0–3 cyclopentane moieties (Schouten et al., 2000; see Appendix 1). They also synthesize crenarchaeol and its regio-isomer with four cyclopentane moieties and a cyclohexane moiety (Sinninghe Damsté et al., 2002; see Appendix 1). *Despite of the fact that archaeal groups other than Thaumarchaeota, e.g. marine Euryarchaeota group II (MG-II), have been proposed to contribute to the isoGDGT signal, this topic is still controversial as no culture representatives of these groups have been obtained yet and thus it is essentially unknown if these groups actually produce isoGDGTs (Lincoln et al., 2014a,b; Schouten et al., 2014). Besides, Thaumarchaeota marine group I are dominant both in marine subsurface and deep waters (e.g. Karner et al., 2001; Herndl et al., 2005; DeLong et al., 2006), where they make up the majority of the archaeal planktonic population. Hence, it is expected that Thaumarchaeota are major contributors of the isoGDGT-signal detected in marine sediments.* Schouten et al. (2002) introduced the TEX_{86} (TetraEther indeX of tetraethers consisting of 86 carbon atoms) as a sea surface temperature (SST) proxy based on the relative abundance of isoGDGTs, excluding GDGT-0 and crenarchaeol. In a follow-up study by Kim et al. (2010), TEX_{86}^{H} has been proposed as a slightly modified version of TEX_{86} with a logarithmic function, which was established based on the core-top dataset, removing the data of the (sub)polar ocean. The TEX_{86}^{H} gave the best correlation for the mesocosm data with temperatures ranging between 10 and 40 °C and for the core-top data with annual mean SSTs between 5 and 30 °C (Kim et al., 2010).

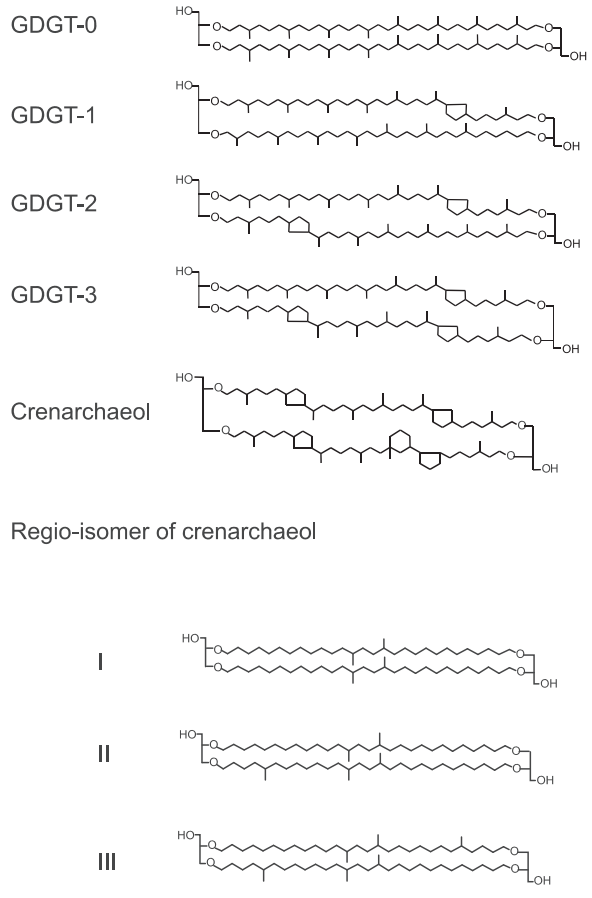

Appendix 1. Chemical structures of isoGDGTs discussed in the text.

Applications of isoGDGT-based indices and the corresponding calibrations in various marine sediment core sites have shown their potential to reconstruct annual mean SSTs, especially where the use of other proxies was limited (e.g. Schouten et al., 2003; Liu et al., 2009; Castañeda et al., 2010; Littler et al., 2011; Bijl et al., 2013). However, it still remains uncertain how well these proxies reconstruct annual mean SSTs due to a number of complicating factors (Schouten et al., 2013 and references therein). For instance, based on the radiocarbon content ($\Delta^{14}C$) of isoGDGTs, it has been suggested that a substantial part of the isoGDGTs in marine sediments are not only derived from surface waters, and that archaeal production in the deeper water column, i.e. below the euphotic zone, may contribute to the signal of isoGDGTs in sediments (e.g. Pearson et al., 2001; Smittenberg et al., 2004; Shah et al., 2008). In addition, recent studies have shown an increase of the isoGDGT with 2 versus 3 cyclopentane moieties (GDGT-2/GDGT-3 ratio) in marine suspended particulate matter (SPM) and surface sediments with increasing water depth (Taylor et al., 2013; Hernández-Sánchez et al., 2014). Consequently, these authors argued that the elevated GDGT-2/GDGT-3 ratios may possibly be due to a substantial contribution of Thaumarchaeota thriving in the deep, bathypelagic water-column. Indeed, Villanueva et al. (2015) observed in a global dataset that the distributional changes of isoGDGTs with increasing water depth coincide with the water depth niches occupied by 'shallow water' (i.e. <200 m water depth) and 'deep water' (i.e. >200 m water depth) Thaumarchaeota based on differences in the thaumarchaeotal ammonia monoxygenase (*amo*A) and in geranylgeranylglyceryl phosphate (GGGP) synthase, an enzyme specifically involved in the isoGDGT biosynthetic pathway. Therefore, it was suggested that differences in the catalytic site of the GGGP synthase between 'shallow water' and 'deep water' Thaumarchaeota could lead to differences in the relative proportion of synthesized isoGDGTs (Villanueva et al., 2014). In a recent study of the Mediterranean Sea, a strong positive relationship between water depth and TEX_{86}^{H} values was observed for both SPM and surface sediments (Kim et al., 2015). Interestingly, an unusually strong decline in the fractional abundance of GDGT-1 with increasing water depth is apparent in the Mediterranean dataset, resulting in a warm bias of TEX_{86}^{H} in deep-water surface sediments. Following the arguments presented above, it was suggested that there might be a change in Thaumarchaeota populations thriving below

the mixed-layer (i.e. surface) waters and that the increasing contribution of membrane lipids of these Thaumarchaeota is, at least partly, responsible for the changing distribution of isoGDGTs in surface sediments. This was confirmed by the isoGDGT distribution of deep water SPM, which was clearly different from that in the surface waters. Enigmatically, however, (i) the contribution of the sub-surface Thaumarchaeota did not further increase in surface sediments from >1000 m water depth, and (ii) temperatures derived of TEX_{86}^{H} values of surface sediments still did show a response to SSTs. This response differs from the global core-top calibration but is similar to that observed in the restricted Red Sea (Kim et al., 2015). Clearly, further study of the influence of sub-surface water dwelling Thaumarchaeota is required for an improved application of the TEX_{86}^{H} paleothermometer in downcore studies.

The western Iberian margin has been a key location for studying the impact and intensity of abrupt glacial climate changes (e.g. Shackleton et al., 2000; Sánchez-Goñi and Harrison, 2010). It has been shown that the Mediterranean Outflow Water (MOW) responded to abrupt climatic changes, affecting the water column stratification on the western Iberian margin (e.g. Voelker and de Abreu, 2011). The applicability of TEX_{86}^{H} has not been thoroughly assessed in this area yet. A question arising is whether the distributions of isoGDGTs along the western Iberian margin might be influenced by the warm and saline, oxygen-depleted MOW. To address these questions, we investigated here SPM ($n = 32$), and surface sediments ($n = 31$) collected in five transects along the southern Portuguese continental margin (Fig. 1). Both core lipid (CL) and intact polar lipid (IPL)-derived isoGDGTs were investigated in order to distinguish more recently produced (IPL-derived) isoGDGTs from older (CL) isoGDGTs, since IPLs are less stable than CLs (e.g. Harvey et al., 1986; Logemann et al., 2011; Xie et al., 2013). We compare these results with the diversity, abundance, and activity data of Thaumarchaeota based on the genetic analysis of the genes coding for the archaeal *amo*A and the thaumarchaeotal GGGP synthase. Using integrated lipid and nucleic acid analyses, our study sheds light on the influence of warm, saline, and oxygen-depleted MOW on deep-water derived isoGDGTs and thus on the isoGDGT-based paleothermometer along the southern Portuguese continental margin.

2. STUDY AREA

The Portuguese continental margin is characterized by a relatively narrow (20 to 34 km wide) shelf (Fig. 1D) and steep irregular slope, incised by several deep canyons (e.g. Nazaré, Cascais, and Lisbon–Setúbal canyons) (e.g. Vanney and Mougenot, 1981). The surface ocean circulation off Portugal is characterized by the Portugal Current (PC), which is a broad and slow southwestward-flowing current from the southeastern side of the North Atlantic Current, with an extension of ~10°W to ~24°W longitude (e.g. Saunders, 1982; van Aken, 2000; Martins et al., 2002) (Fig. 1A). During the summer upwelling season (May to September), the Portugal Coastal Current (PCC) flows southward induced by the northerly Portuguese trade winds blowing nearly parallel to the coast (e.g. Fiúza et al., 1982; Martins et al., 2002). During the winter downwelling season (October to April), the surface circulation reverses becoming the poleward flowing Portugal Coastal Countercurrent (PCCC) predominant close to the coast (e.g. Ambar and Fiúza, 1994) (Fig. 1A). Annual mean temperature and salinity in surface water decrease from South to North, varying between 19 and 15 °C (Fig. 1B) and between 36.4 and 35.6 (Fig. 1C), respectively. The Eastern North Atlantic Central Water (ENACW) occurs at water depths between 100 m and 500 m. The warmer and more saline subtropical ENACW is formed along the Azores front during winter at 35–36°N, while the subpolar ENACW, which flows below the subtropical ENACW, is formed by winter cooling in the eastern North Atlantic north of 46°N (e.g. Fiúza et al., 1998). Below the ENACW, the MOW is of central importance for the circulation in the region. The MOW is known to be formed by the outflow of highly dense Mediterranean water across the Strait of Gibraltar (main sill depth of 280 m) and the subsequent entrainment of less dense overlying ENACW through the Gulf of Cadiz (e.g. Baringer and Pricem, 1997). The MOW consists of changeable parts of Levantine Intermediate Water (LIW) and Western Mediterranean Deep Water (WMDW) (e.g. Kinder and Parrilla, 1987). The LIW and the WMDW are formed near Rhodes and in the Gulf of Lions (South of France) in winter when outbursts of cold, dry air from the European continent induce surface water cooling and deep convection in the eastern basin (the Levantine, the Aegean, the Adriatic) and in the western basin (the Liguro-Provencal), respectively (e.g. Candela, 2001). The LIW at 200–600 m water depth is the warmest and saltiest waters in the Mediterranean Sea, with temperatures of ~13.0–13.4 °C and salinities of ~38.48–38.55 (e.g. Bryden and Stommel, 1982; Puig et al., 2013). Pure WMDW is recognized below ~2000 m in the Liguro-Provencal with T ~12.75–12.82 °C and S ~38.43–38.47 (e.g. van Haren and Millot, 2004; Puig et al., 2013). Possibly along with the variable bottom topography, the MOW splits into two major core layers: the Mediterranean Upper Water centered at ca. 500−800 m and the more saline and denser Mediterranean Lower Water at ca. 1000−1600 m. Below the MOW, the Antarctic Intermediate Water (AAIW) flows in a northward direction, which is underlain by the Northeast Atlantic Deep Water (NEADW) flowing southward (van Aken, 2000).

3. MATERIALS AND METHODS

3.1. Multibeam and seismic surveying

The PACEMAKER 64PE332 cruise was conducted with the R/V Pelagia between 14th and 29th March 2011. Five transect sites (Fig. 1D) were surveyed simultaneously with a Kongsberg EM300 multibeam sea bathymetry system of R/V Pelagia and with a seismic reflection system from Geo-Marine Survey Systems. Survey speed was 5−6 nm h^{-1}. The sparker system consisted of a Geo-Source 200 tip sparker source with a 1 kJ Geo-spark pulsed power supply. The signal frequency bandwidth ranged from

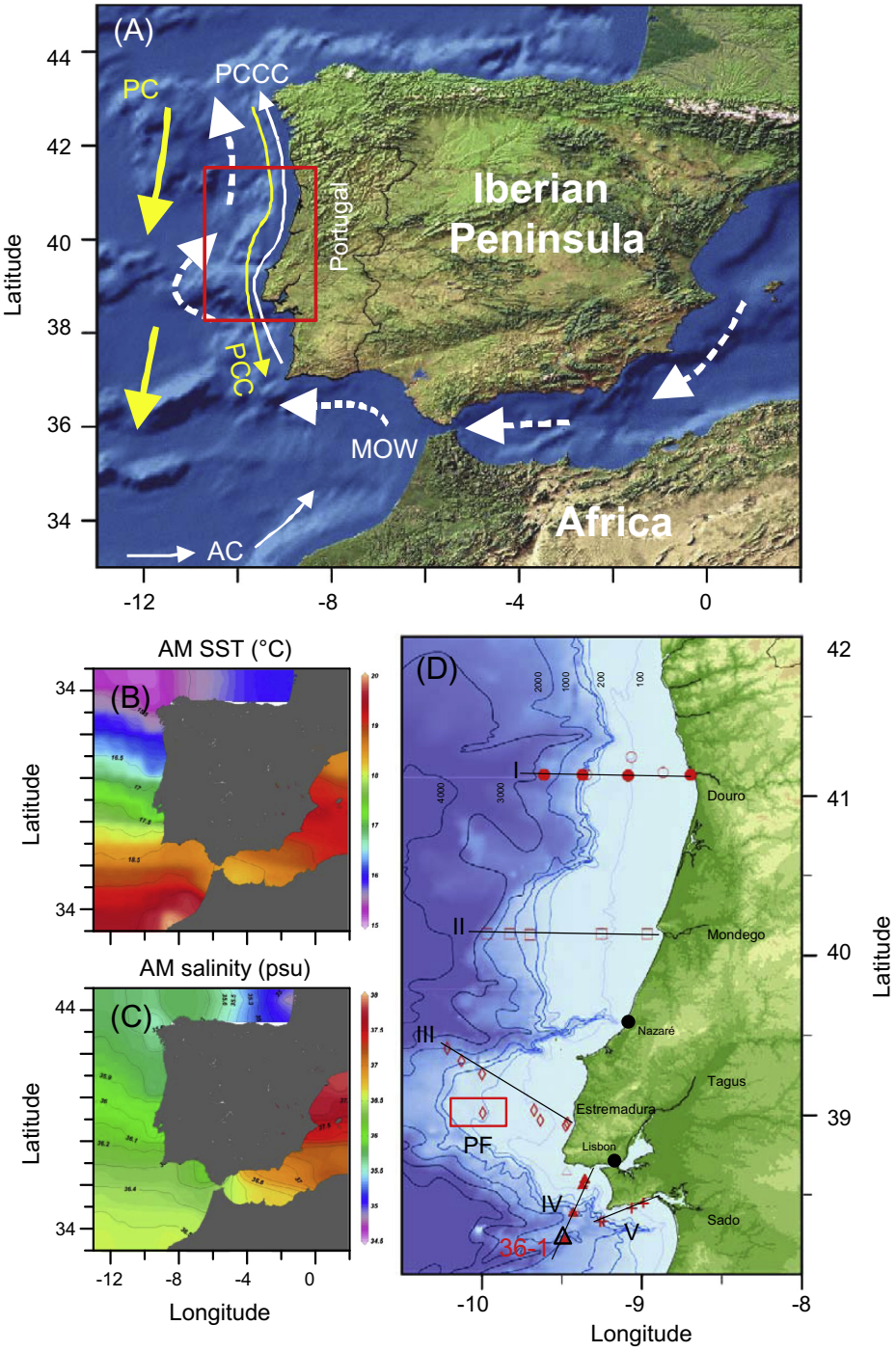

Fig. 1. (A) Overview of the study area with the current system. Major current and water masses are indicated: PC Portugal Current, PCC Portugal Coastal Current, PCCC Portugal Coastal Countercurrent, MOW Mediterranean Outflow Water, and AC Azores Current. Distribution of (B) annual mean SST and (C) annual mean salinity off the Iberian margin (based on the world ocean atlas 13 (WOA13) dataset (Locarnini et al., 2013; Zweng et al., 2013). (D) Location of the stations for sampling of surface sediments along the five (I: Douro, II: Mondego, III: Estremadura, IV: Tagus, and V: Sado) transects. Filled symbols indicate the stations at which SPM was also sampled. The open black triangle indicates station 36-1 where SPM for molecular ecology were sampled. PF indicates "pockmark field".

500 Hz to 3500 Hz corresponding to decimetre resolution, especially in the upper 20 m of sediments. The sparker profiles acquired during this survey had an average signal penetration of 100 m below the seafloor.

3.2. Measurement of physical and chemical parameters

To obtain information on the physical parameters of the water masses in the study area, a conductivity–tempera

ture–depth (CTD) system was employed. The CTD profiling of the water column down to a maximum water depth of 2500 m was conducted using a Sea-Bird "SBE-9+" underwater unit, a Sea-Bird "SBE-11+" deck unit, a SBE-4 conductivity sensor, a SBE-3 temperature sensor, a SBE-43 dissolved oxygen sensor, a Wetlabs C-star 25 cm transmissometer, a Chelsea Technology Aquatracka III fluorometer, and a bottom sensing altimeter. Altimeter tracks the bottom from 20 m to 50 m height, depending on sediment type. The vertical profile provided data for temperature, salinity, dissolved oxygen, fluorescence (chlorophyll), and turbidity (Fig. 2; see also Appendixes 2 and 3). Satellite-derived SST data for each sampling station were obtained following methods described by Kim et al. (2010).

A rosette system with a Sea-Bird SBE 32 sampler carousel and a NIOZ hexagon frame with 16 × 12 L Niskin bottles was attached to the CTD. Samples for seawater nutrient analysis were taken from the Niskin bottles into polypropylene bottles and ca. 5 mL samples were filtered over 0.45 μm × 25 mm Acrodisc HT Tuffryn Membrane syringe filters (Pall Corporation, Washington) into pre-rinsed pony vials. The samples were sub-sampled in a 5 mL polyethylene vial. Samples analyzed onboard were stored dark at −20 °C and were analyzed during the next cruise 64PE334 STRATIPHYT (07/04/2011 to 04/05/2011) on a QuAAtro auto-analyzer. The standard deviation of samples measured between different runs was NH_4^+ 0.06 μM; $NO_3^- + NO_2^-$ 0.06 μM; and NO_2^- 0.01 μM.

3.3. Sample collection

For the GDGT analysis, SPM samples were collected at four stations along the Douro (I) and Tagus (IV) transects at two to five different water depths (Table 1; Fig. 1D). Between 60 and 240 L of seawater were filtered over pre-ashed glass-fiber filters (Whatman GF/F, 142 mm diameter, 0.7 μm pore size) with two McLane *in situ* pump system (McLane Laboratories Inc., Falmouth, MA). All SPM samples were kept frozen immediately at −20 °C on board. The nominal pore size of the filters is slightly larger than thaumarchaeotal cells (typically <0.6 μm; Könneke et al., 2005). However, the effective pore size decreases during the filtration, and previous studies have shown that the concentration profiles of isoGDGTs obtained from 0.7 μm filters correspond well with those of thaumarchaeotal DNA obtained from 0.2 μm filters and that a representative fraction of archaea is still retained on the 0.7 μm filters (e.g. Herfort et al., 2007; Schouten et al., 2012).

Sediment cores were retrieved at 30 stations at transects I–V (Table 2; Fig. 1D) using the MUC 8+4 multi-corer developed by Oktopus GmbH, which was equipped with an array of eight 6-cm diameter and four 10-cm diameter polycarbonate coring tubes of 61 cm length. In addition, a box corer with a cylindrical coring barrel of 30 cm diameter and 55 cm length was deployed at station 26-2. The sediment cores were sliced using a hydraulic slicer, and all the samples were immediately stored at −20 °C after sampling. Upon arrival in the laboratory, SPM filters, and sediment samples were stored at −40 °C until freeze drying and extraction. The 0–0.5 cm layer (surface sediment) of the cores was used in this study.

For the nucleic acid analyses, another set of the SPM samples (see the description above) was taken at the Tagus transect station 36-1 (1989 m water depth; Table 1, see also Fig. 1D) at the same water depths where the GDGT SPM samples were collected.

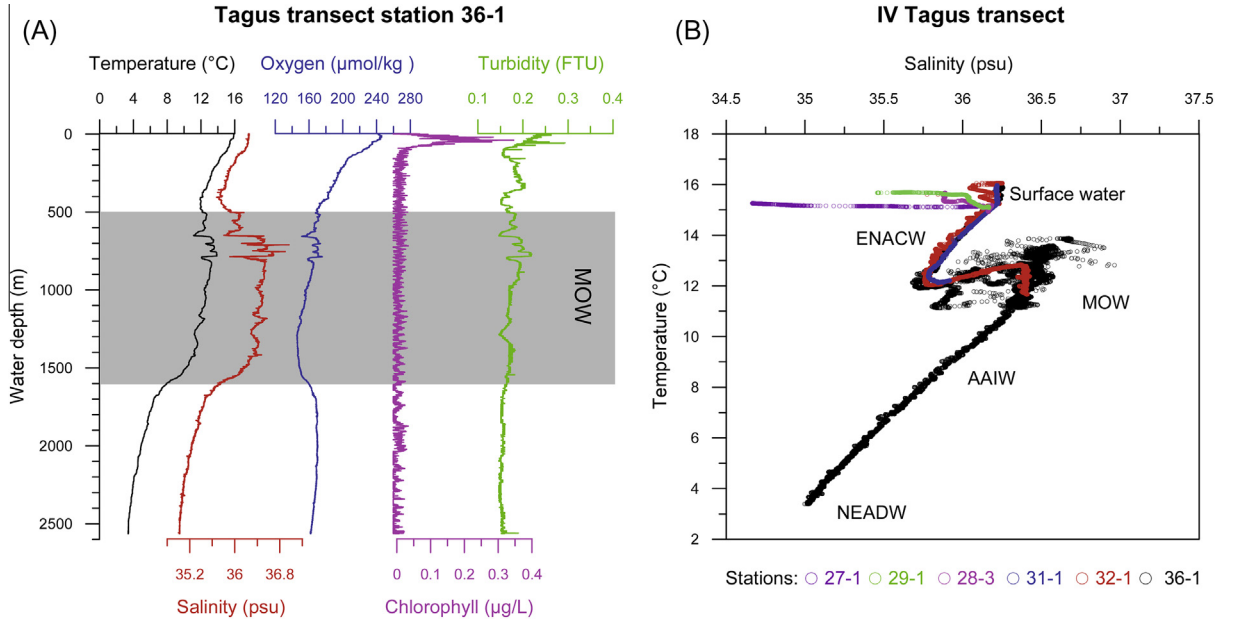

Fig. 2. (A) CTD profile of temperature (°C), (B) salinity (psu), (C) oxygen concentration (μmol/kg), chlorophyll concentration (μg/L, as measured by fluorometer), and turbidity (FTU) at station 36-1. (B) Temperature and salinity (T–S) plot of CTD data obtained from the Tagus transect. Major water masses are indicated: ENACW Eastern North Atlantic Central Water, MOW Mediterranean Outflow Water, AAIW Antarctic Intermediate Water, NEADW Northeast Atlantic Deep Water.

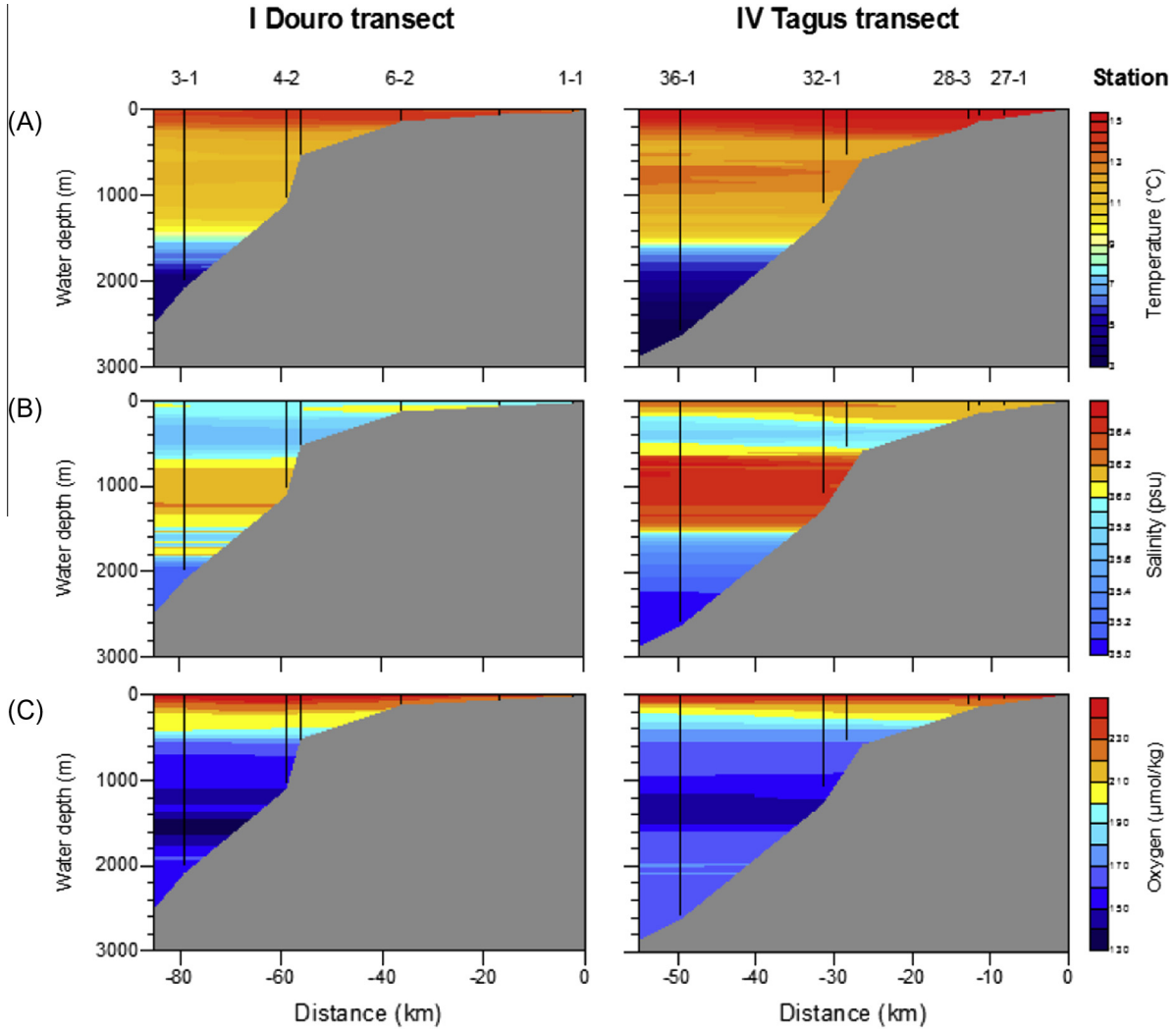

Appendix 2. Vertical distribution pattern of (A) temperature (°C), (B) salinity (psu), and (C) oxygen concentration (μmol/kg) obtained from the CTD data along the Douro and Tagus transects. The CTD sites are indicated by black lines.

3.4. GDGT extraction and analysis

Extraction and purification procedure of CL and IPL-derived GDGTs for SPM filters and surface sediments were carried out as described by Zell et al. (2014). Briefly, the freeze-dried SPM filters and ten selected surface sediments collected along the Douro ($n = 5$) and Tagus ($n = 5$) transects were extracted with a modified Bligh and Dyer (BD) technique and fractioned into CLs and IPLs over an activated silica gel (Pitcher et al., 2009). For the GDGT quantification, 0.01 μg C_{46} GDGT internal standard was added to the CL and IPL fractions. The CL fractions of the BD extracts were separated into three fractions over an Al_2O_3 column (activated for 2 h at 150 °C) using hexane:dichloromethane (DCM; 9:1, v:v), hexane:DCM (1:1, v:v), and DCM:methanol (MeOH; 1:1, v:v), respectively. Part of the IPL fraction was hydrolyzed to obtain IPL-derived CLs. It was reported by Pitcher et al. (2009) that during the separation between CL and IPL fraction a small amount of the CL GDGTs may be carried over into the IPL fraction. Therefore, the DCM:MeOH fraction from the original CL fractions, the hydrolyzed IPL fractions (IPL-derived fraction), and the non-hydrolyzed IPL fractions were analyzed to implement a correction more accurately to calculate the amounts of CL and IPL-derived isoGDGTs as described by Weijers et al. (2011a).

All surface sediments (ca. 0.3–3 g) were extracted with an Accelerated Solvent Extractor (ASE). The internal standard C_{46} GDGT (0.1 μg) was added to the total extracts for the GDGT quantification. The ASE extracts were separated into two fractions over an Al_2O_3 column (activated for 2 h at 150 °C) using hexane:DCM (1:1, v:v) and DCM:MeOH (1:1, v:v), respectively. The polar DCM:MeOH fraction was analyzed for CL isoGDGTs.

All samples were analyzed using a high performance liquid chromatography–atmospheric pressure positive ion chemical ionization–mass spectrometry (HPLC–APCI–MS) according to the method described by Schouten et al. (2007). The analytical error was determined by duplicate measurements of six samples. The concentrations had a

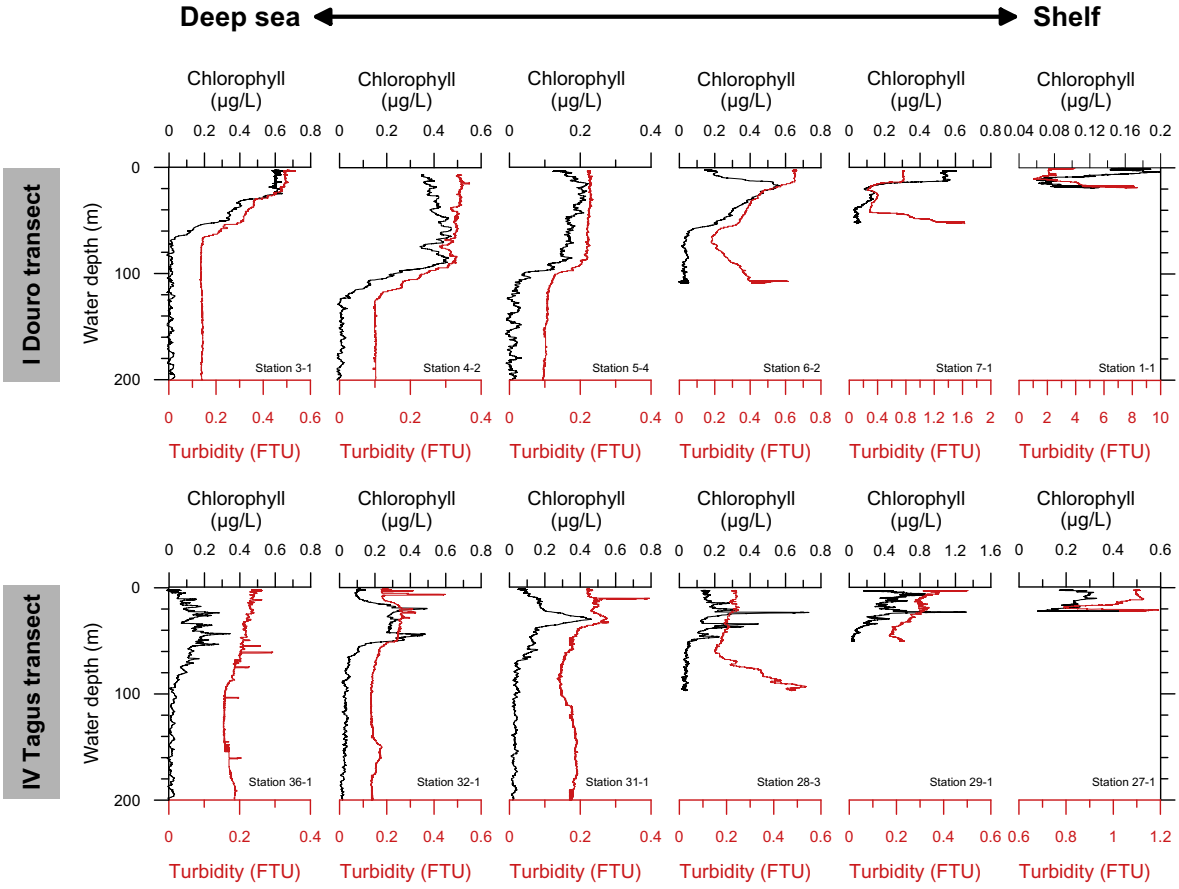

Appendix 3. Vertical profiles of chlorophyll concentration (µg/L, as measured by a fluorometer) and turbidity (FTU) in the upper 300 m of the water column along the Douro and Tagus transects.

standard deviation of 17% for the CL isoGDGTs and 10% for the IPL-derived isoGDGTs.

The TEX_{86}^{H} was calculated according to Kim et al. (2010) and TEX_{86}^{H} values were converted into temperature values using the global core-top calibration for satellite-derived annual mean SST (Kim et al., 2010):

$$TEX_{86}^{H} = \log(TEX_{86}^{H}) = \log\left(\frac{[GDGT-2]+[GDGT-3]+[Cren']}{[GDGT-1]+[GDGT-2]+[GDGT-3]+[Cren']}\right) \quad (1)$$

$$T = 68.4 \times TEX_{86}^{H} + 38.6 (r^2 = 0.87, n = 255, p < 0.0001) \quad (2)$$

$$\text{BIT index} = \frac{[I]+[II]+[III]}{[I]+[II]+[III]+[Cren]} \quad (3)$$

GDGT-1, GDGT-2, and GDGT-3 indicate isoGDGTs containing 1, 2, and 3 cyclopentane moieties, respectively (see Appendix 1). The Roman numerals (I, II, and III) refer to branched GDGTs while Cren and Cren' indicate crenarchaeol and its regio-isomer, respectively (see Appendix 1).

3.5. Nucleic acid (RNA and DNA) extraction and analysis

One quarter of the GF/F filters (142 mm diameter, 0.7 µm pore size) containing the SPM of the Tagus transect station 36-1 at 1 m, 50 m, and 200 m water depth (for the 1000 m water depth sample, the entire filter was used) were cut into small pieces before extraction. DNA/RNA was extracted from the SPM filters with the RNA PowerSoil® Total Isolation kit plus the DNA elution accessory (Mo Bio Laboratories, Inc., Carlsbad, CA, USA) with a final volume of 60 µl for both DNA and RNA extracts. RNA extracts were treated with DNAse and reverse transcribed as described by Pitcher et al. (2011). Quantitative PCR of the Thaumarchaeota (formerly marine crenarchaeota group I, MCGI) 16S rRNA gene and *amo*A gene in SPM samples was performed as described by Pitcher et al. (2011).

Amplification of the archaeal *amo*A gene was performed as described by Yakimov et al. (2011) following the conditions described in Villanueva et al. (2015). A fragment of the thaumarchaeotal GGGP synthase coding gene was amplified as described in Villanueva et al. (2015). PCR products were gel purified (QIAquick gel purification kit, Qiagen, Valencia, CA, USA) and cloned in the TOPO-TA cloning® kit from Invitrogen (Carlsbad, CA, USA) and transformed into *E. coli* TOP10 cells following the manufacturer's recommendations. Recombinant clones plasmid DNAs were purified and sequenced by Baseclear (Leiden, The Netherlands). The archaeal *amo*A and thaumarchaeotal GGGP synthase sequences were translated into protein sequences, which were aligned with already annotated

Table 1
SPM samples studied and their general properties.

Sample name	Cruise	Station	Longitude	Latitude	Sampling date (dd/mm/yyyy)	Sampling water depth (m)	SPM (mg/L)	Satellite-derived AM SST (°C)	In-situ temperature (°C)	Distance from the coast (km)	NH4 (μM)	NO2 (μM)	NO3 (μM)
I. Douro transect													
64PE332-1-1-1 m	64PE332	1-1	−8.69	41.13	14/03/2011	1	11.9	14.8	12.1	2.3	2.3	0.6	53.1
64PE332-1-1-14 m						14	9.6	14.8	13.8	2.3	0.5	0.3	7.2
64PE332-6-2-1 m	64PE332	6-2	−9.08	41.13	17/03/2011	1	1.9	15.5	14.1	36.4	0.2	0.2	0.6
64PE332-6-2-20 m						20	0.8	15.5	13.9	36.4	0.2	0.2	1.5
64PE332-6-2-50 m						50	1.0	15.5	14.0	36.4	0.2	0.2	2.5
64PE332-6-2-109 m						109	1.4	15.5	14.3	36.4	0.2	0.1	4.7
64PE332-4-2-1 m	64PE332	4-2	−9.37	41.13	16/03/2011	1	0.6	16.0	14.0	58.9	0.3	0.4	2.0
64PE332-4-2-50 m						50	1.9	16.0	14.0	58.9	0.3	0.4	2.4
64PE332-4-2-200 m						200	1.0	16.0	13.6	58.9	0.2	0.0	7.8
64PE332-4-2-500 m						500	0.2	16.0	11.6	58.9	0.1	0.0	13.2
64PE332-4-2-1006 m						1006	0.2	16.0	11.4	58.9	0.1	0.0	15.4
64PE332-3-1-1 m	64PE332	3-1	−9.61	41.14	15-16/03/2011	1	0.6	16.3	13.9	79.0	0.3	0.2	1.9
64PE332-3-1-50 m						50	0.7	16.3	14.0	79	0.2	0.3	2.2
64PE332-3-1-200 m						200	0.3	16.3	12.8	79.0	0.1	0.0	8.8
64PE332-3-1-1000 m						1000	0.6	16.3	11.2	79	0.2	0.0	15.6
64PE332-3-1-1988 m						1988	0.8	16.3	4.4	79.0	0.3	0.0	16.9
IV. Tagus transect													
64PE332-27-1-1 m	64PE332	27-1	−9.36	38.61	24/03/2011	1	2.3	16.0	15.7	8.7	0.6	0.4	3.8
64PE332-27-1-19 m						19	2.3	16.0	15.5	8.7	0.5	0.4	2.5
64PE332-28-3-1 m	64PE332	28-3	−9.37	38.56	24/03/2011	1	0.6	16.4	15.6	12.8	0.3	0.1	0.2
64PE332-28-3-20 m						20	0.9	16.4	15.3	12.8	0.4	0.1	0.3
64PE332-28-3-50 m						50	0.6	16.4	15.1	12.8	0.3	0.4	2.3
64PE332-28-3-93 m						93	1.0	16.4	15.0	12.8	0.3	0.6	2.6
64PE332-32-1-1 m	64PE332	32-1	−9.43	38.39	25/03/2011	1	0.5	16.7	16.1	31.3	0.3	0.0	0.0
64PE332-32-1-50 m						50	0.4	16.7	15.4	31.3	0.3	0.4	0.8
64PE332-32-1-200 m						200	0.8	16.7	14.4	31.3	0.2	0.1	6.9
64PE332-32-1-500 m						500	0.4	16.7	12.1	31.3	0.2	0.0	13.1
64PE332-32-1-1051 m						1051	0.7	16.7	11.7	31.3	0.3	0.0	13.7
64PE332-36-4-1 m	64PE332	36-4	−9.48	38.23	27/03/2011	1	0.4	17.0	15.9	49.6	0.4	0.0	0.1
64PE332-36-4-50 m						50	0.4	17.0	15.4	49.6	0.3	0.4	1.1
64PE332-36-4-200 m						200	0.8	17.0	13.9	49.6	0.1	0.0	6.7
64PE332-36-4-1000 m						1000	1.0	17.0	12.4	49.6	0.1	0.0	10.9
64PE332-36-4-2431 m						2431	0.6	17.0	3.5	49.6	0.2	0.0	18.8

Table 2
Surface sediment samples studied and their general properties.

Sample name	Cruise	Station	Longitude	Latitude	Water depth (m)	Coring device	Sampling date (dd/mm/yyyy)	Satellite-derived AM SST (°C)
I. Douro transect								
64PE332-1-3	64PE332	1-3	−8.69	41.13	15	Multicorer	14/03/2011	14.8
64PE332-7-2	64PE332	7-2	−8.87	41.15	51	Multicorer	17/03/2011	15.3
64PE332-9-1	64PE332	9-1	−9.07	41.24	104	Multicorer	18/03/2011	15.4
64PE332-6-1	64PE332	6-1	−9.08	41.13	110	Multicorer	17/03/2011	15.5
64PE332-5-2	64PE332	5-2	−9.34	41.14	506	Multicorer	17/03/2011	15.9
64PE332-4-1	64PE332	4-1	−9.37	41.13	1007	Multicorer	16/03/2011	16.0
64PE332-3-7	64PE332	3-7	−9.61	41.14	1989	Multicorer	16/03/2011	16.3
II. Mondego transect								
64PE332-11-2	64PE332	11-2	−8.97	40.13	28	Multicorer	19/03/2011	15.3
64PE332-12-1	64PE332	12-1	−9.25	40.13	108	Multicorer	19/03/2011	16.2
64PE332-13-3	64PE332	13-3	−9.70	40.13	505	Multicorer	19/03/2011	16.6
64PE332-14-4	64PE332	14-4	−9.83	40.13	981	Multicorer	19/03/2011	16.8
64PE332-15-1	64PE332	15-1	−9.97	40.13	1808	Multicorer	20/03/2011	16.9
III. Estremadura transect								
64PE332-24-2	64PE332	24-2	−9.47	38.95	41	Multicorer	23/03/2011	15.9
64PE332-17-2	64PE332	17-2	−9.48	38.93	48	Multicorer	21/03/2011	16.0
64PE332-18-5	64PE332	18-5	−9.67	39.03	116	Multicorer	21/03/2011	16.2
64PE332-25-2	64PE332	25-2	−9.64	38.97	119	Multicorer	23/03/2011	16.2
64PE332-26-2	64PE332	26-2	−10.00	39.01	259	Boxcorer	23/03/2011	16.8
64PE332-20-2	64PE332	20-2	−10.00	39.26	308	Multicorer	21/03/2011	16.8
64PE332-22-6	64PE332	22-6	−10.13	39.34	1100	Multicorer	22/03/2011	17.0
64PE332-23-2	64PE332	23-2	−10.22	39.42	1980	Multicorer	22/03/2011	17.1
IV. Tagus transect								
64PE332-27-3	64PE332	27-3	−9.36	38.61	20	Multicorer	24/03/2011	16.0
64PE332-29-2	64PE332	29-2	−9.36	38.58	48	Multicorer	25/03/2011	16.2
64PE332-30-1	64PE332	30-1	−9.47	38.65	81	Multicorer	25/03/2011	16.0
64PE332-28-1	64PE332	28-1	−9.37	38.56	94	Multicorer	24/03/2011	16.4
64PE332-31-2	64PE332	31-2	−9.42	38.42	478	Multicorer	25/03/2011	16.6
64PE332-33-1	64PE332	33-1	−9.43	38.39	1052	Multicorer	26/03/2011	16.7
64PE332-36-3	64PE332	36-3	−9.48	38.23	2432	Multicorer	27/03/2011	17.0
V. Sado transect								
64PE332-34-2	64PE332	34-2	−8.99	38.45	48	Multicorer	26/03/2011	16.4
64PE332-38-2	64PE332	38-2	−9.06	38.42	98	Multicorer	28/03/2011	16.7
64PE332-37-2	64PE332	37-2	−9.24	38.34	516	Multicorer	28/03/2011	16.7
64PE332-40-1	64PE332	40-1	−9.26	38.33	979	Multicorer	28/03/2011	16.7

sequences by using the Muscle application (Edgar, 2004). Phylogenetic trees were constructed with the Neighbor-Joining method (Saitou and Nei, 1987) and evolutionary distances computed using the Poisson correction method with a bootstrap test of 1000 replicates. *Amo*A sequences obtained in this study were also added to the *amo*A gene sequence (DNA-based) reference tree provided by Pester et al. (2012) based on 592 unambiguously aligned nucleotides using the parsimony interactive tool of ARB (Ludwig et al., 2004). Partial GGGP synthase and *amo*A gene sequence data are deposited in the NCBI GenBank database under accession No: KP75439−KP754462 and KP754236−KP754358, respectively.

4. RESULTS

4.1. Physicochemical properties

At the time of sampling, the water masses in the study area were characterized by a temperature range of 3–16 °C, a salinity range of 34.5–37.0 practical salinity units (psu), and a range in oxygen content of 130–250 μmol/kg (Fig. 2A; see also Appendix 2). A temperature and salinity (T–S) plot revealed the presence of the different water masses in the study area: surface water, ENACW, MOW, AAIW, and NEADW (Fig. 2B). The influence of fresher river waters was reflected by lower salinity values of the surface water on the shelf. Coastal upwelling was not observed at the time of the cruise. A warm surface water layer of up to ~100 m thick was underlain by a steep thermocline at the offshore stations. Below the thermocline, a clear rise in salinity and temperature accompanied by a decrease in oxygen concentration marked the boundaries between ENACW and MOW at about 500 m water depth and between MOW and AAIW at around 1600 m water depth (Fig. 2A). NEADW was located deeper down (i.e. ~2100 m) in the water column.

The CTD profiles showed that waters with high turbidity values corresponded to high chlorophyll concentration, as measured by fluorometry, in the upper 100 m of the

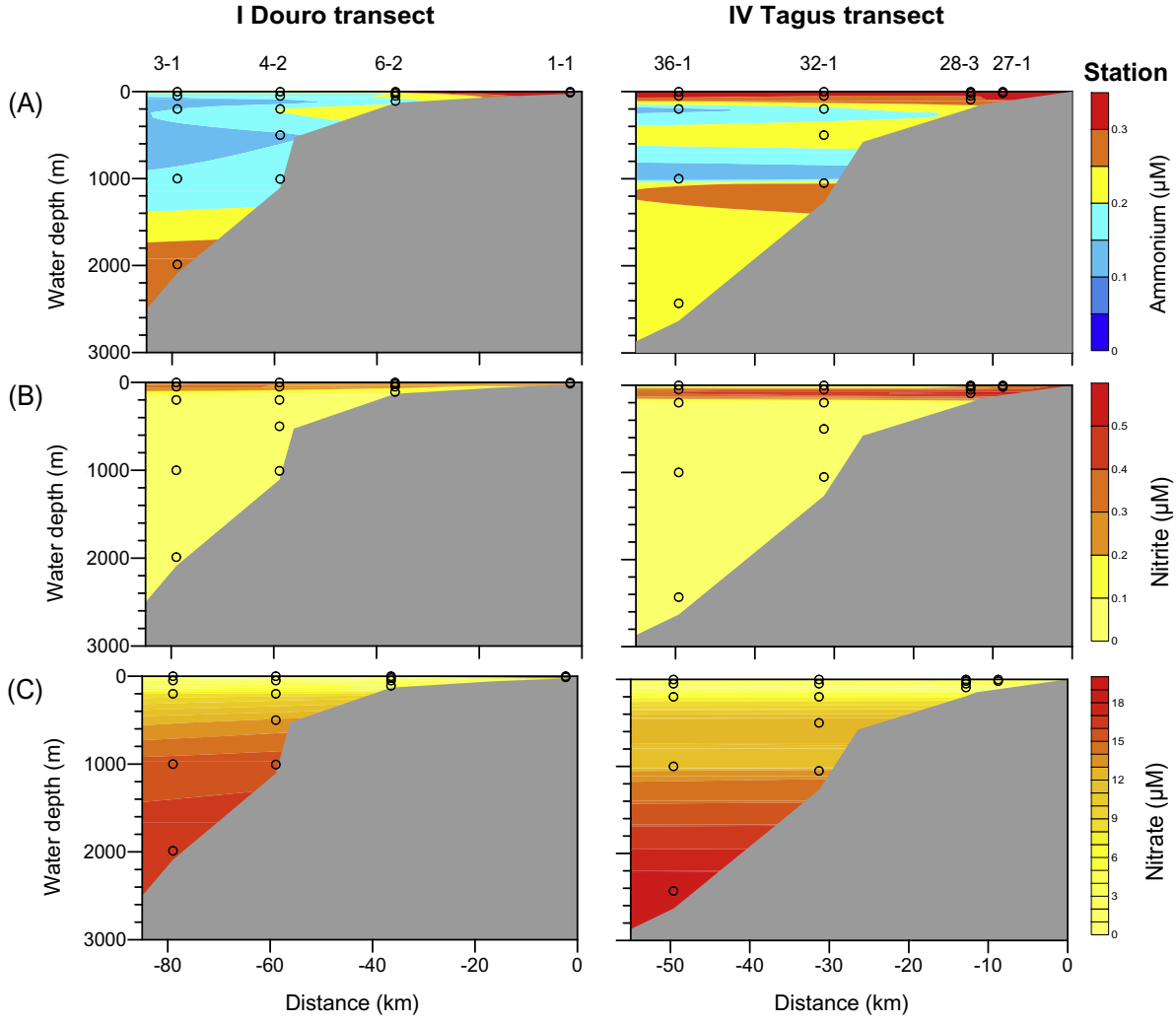

Appendix 4. Vertical and spatial distribution patterns of (A) the ammonium (NH_4^+, μM), (B) nitrite (NO_2^-, μM), and (C) nitrate (NO_3^-, μM) concentration along the Douro and Tagus transects. Open circles indicate the sampling depth.

water column at the offshore sites, indicating higher amounts of fresh phytoplankton (Fig. 2A; see also Appendix 3). The chlorophyll concentration usually displayed a maximum around 20–50 m water depth in the most offshore stations and at progressively shallower water depths (i.e. up to <10 m) near the coast. Below the upper layers of the water column, where primary productivity took place, enhanced turbidity was observed in bottom water layers on the shelf, which was caused by resuspension of sediment from the seabed. Ammonium concentrations in the water column ranged from 0.1 μM to 2.3 μM (Table 1; see also Appendix 4). The nitrite and nitrate concentrations varied between <0.01 μM (i.e. below the detection limit) and 0.6 μM and between <0.01 μM (i.e. below the detection limit) and 53 μM, respectively (Table 1; see also Appendix 4).

4.2. IsoGDGT concentrations and distributions in SPM

In the SPM, the summed concentration of all six isoGDGTs normalized on organic carbon (OC) was 30–650 μg/gOC for the CL fraction (see Appendix 5). The most abundant CL isoGDGTs were GDGT-0 (fractional abundance of 40 ± 7%) and crenarchaeol (48 ± 2%) with average concentrations of 90 ± 70 μg/gOC and 100 ± 80 μg/gOC, respectively. The summed concentration of four isoGDGTs used for the calculation of the TEX_{86}^{H} was 2 to 129 μg/gOC with an average value of 27 ± 25 μg/gOC for the CL fraction (see Appendix 5). The IPL-derived GDGT-0 and crenarchaeol relative to the total (i.e. CL and IPL-derived) amount of isoGDGTs were on average 10 ± 6% and 8 ± 4%, respectively. The IPL-derived four isoGDGTs used for the TEX_{86}^{H} comprised on average 7 ± 5% of the total amount of isoGDGTs. In general, the Douro and Tagus transects showed different patterns in CL concentration for both crenarchaeol and four isoGDGTs used for the TEX_{86}^{H} (Fig. 3A and C). For the Douro transect, the highest concentrations were observed in the deepest water at station 3-1 (Fig. 3C), while the concentrations were generally higher below the surface mixed layer for the Tagus transect (Fig. 3A). The IPL-derived percentages of crenarchaeol and four isoGDGTs were generally higher below the surface mixed layer within the euphotic zone in both transects (Fig. 3B and D). Pronounced maxima also occurred at 1000 m water depth for both transects, especially for the four isoGDGTs used for the TEX_{86}^{H} (Fig. 3B and D).

The distribution of the four isoGDGTs used for the calculation of the TEX_{86}^{H} varied throughout the water column for both CL and IPL-derived isoGDGTs (Fig. 4). The most notable difference between CL and IPL-derived isoGDGTs was observed in SPM collected at a water depth range of 500–1600 m, with an increasingly higher fractional abundance of GDGT-2 and the crenarchaeol regio-isomer but lower fractional abundance of GDGT-1 with increasing depth, especially for the IPL-derived isoGDGTs (Fig. 4). Accordingly, much higher TEX_{86}^{H} values and thus temperatures reconstructed using the global core-top calibration (Eq. (2)) were obtained between 500 m and 1600 m water depth for the isoGDGTs (Fig. 5). The TEX_{86}^{H} values (Fig. 5A) were generally higher for the IPL-derived isoGDGTs (−0.33 to −0.04) than for the CL isoGDGTs (−0.48 to −0.16). TEX_{86}^{H} -derived temperatures (Fig. 5B) were thus substantially higher for the IPL-derived isoGDGTs (16–36 °C) than for the CL isoGDGTs (6–28 °C).

4.3. IsoGDGT concentrations and distributions in marine surface sediments

The concentrations of all six CL isoGDGTs in the surface sediments, as obtained by ASE extraction, varied between 300 and 2600 μg/gOC in the surface sediments (Appendix 6). The most common CL isoGDGTs were GDGT-0 (39 ± 5%) and crenarchaeol (48 ± 2%) with average concentrations of 350 ± 190 μg/gOC and 430 ± 230 μg/gOC, respectively. The relative proportion of four CL isoGDGTs used for the TEX_{86}^{H} calculation was comparatively low (13 ± 4%), with varying summed concentrations between 30 and 350 μg/gOC (Appendix 6). The analysis of the multibeam data allowed the identification of more than 30 pockmarks in the Estremadura Spur (see Appendix 7). Notably, the highest concentrations of CL crenarchaeol and four CL isoGDGTs were found in the pockmarks field (Fig. 6A and B, see also Fig. 1D). The CL TEX_{86}^{H} varied between −0.36 and −0.19 (Fig. 6C). The CL TEX_{86}^{H} -derived temperatures were in the range of 14–25 °C (Fig. 6D). The fractional abundances of CL GDGT-2 and CL crenarchaeol regio-isomer were higher in surface sediments from deeper water, while those of CL GDGT-1 and CL GDGT-3 were lower (Fig. 4). Consequently, the CL TEX_{86}^{H} and the reconstructed temperatures did show an increasing trend in an offshore direction with increasing water depths (Fig. 6C and D).

For the ten surface sediments of the Douro and Tagus transects (Fig. 1) IPL-derived isoGDGTs were also measured using the BD extraction method used for the SPM. The CL concentrations of four isoGDGTs used for the TEX_{86}^{H} obtained by BD extraction were 7–66 μg/gOC (on average 35 ± 19 μg/gOC), while those of the ASE extraction for the same samples were 34–143 μg/gOC (on average 90 ± 37 μg/gOC) (see Appendix 6). Hence, the CL concentrations determined using the BD extraction were, in general, lower than those obtained by the ASE extraction. The CL TEX_{86}^{H} and reconstructed temperatures using the global core-top calibration (Eq. (2)) were on average 0.014 and 0.9 °C, respectively, slightly lower in the BD extracts than in the corresponding ASE extracts. However, the differences due to the different extraction methods were negligible as found by Lengger et al. (2012). The percentage of IPLs of the total isoGDGT amount was on average 4 ± 2 for GDGT-0, 3 ± 1 for crenarchaeol, and 2 ± 1 for four isoGDGTs used for the TEX_{86}^{H} (see Appendix 6). The distribution of IPL-derived isoGDGTs varied with water depth, comparable as determined for CL isoGDGTs (Fig. 4). The TEX_{86}^{H} and reconstructed temperatures for the IPL-derived isoGDGTs ranged from −0.280 to −0.209, corresponding to 19–24 °C.

Appendix 5
Concentrations of CL and IPL-derived isoGDGTs normalized to OC and BIT values for SPM obtained by the BD extraction.

Sample name	Fraction	C1302 (μg/gOC)	C1300 (μg/gOC)	C1298 (μg/gOC)	C1296 (μg/gOC)	C1292 (μg/gOC)	C1292' (μg/gOC)	Sum of all 6 CL isoGDGTs (μg/gOC)	Sum of 4 CL isoGDGTs (μg/gOC)	BIT	Comments
64PE332-1-1-1 m	CL	83	8	4	2	69	1	167	15	0.26	
64PE332-1-1-14 m	CL	227	26	16	7	310	23	609	72	0.07	
64PE332-6-2-1 m	CL	36	3	1	0.4	32	0.3	72	4	0.04	
64PE332-6-2-20 m	CL	142	11	3	1	132	0.4	291	16	0.01	
64PE332-6-2-50 m	CL	257	21	7	3	249	2	539	33	0.01	
64PE332-6-2-109 m	CL	170	22	11	5	185	3	397	42	0.02	
64PE332-4-2-1 m	CL	93	9	4	2	89	1	199	16	0.00	
64PE332-4-2-50 m	CL	64	7	3	1	79	1	155	13	0.00	
64PE332-4-3-200 m	CL	93	16	11	3	117	5	246	36	0.00	
64PE332-4-2-500 m	CL	52	13	13	2	92	6	178	34	0.00	
64PE332-4-4-1006 m	CL	35	10	13	1	56	5	120	29	0.01	
64PE332-3-2-1 m	CL	36	3	2	1	34	0.4	76	6	0.00	
64PE332-3-1-50 m	CL	62	12	6	3	93	3	178	24	0.00	
64PE332-3-3-200 m	CL	65	11	8	2	79	2	168	24	0.00	
64PE332-3-1-1000 m	CL	16	6	8	1	38	4	73	19	0.00	
64PE332-3-4-1988 m	CL	212	48	53	6	306	22	647	129	0.01	
64PE332-27-1-1 m	CL	110	10	5	2	104	1	232	17	0.18	
64PE332-27-1-19 m	CL	82	8	4	2	83	2	181	16	0.17	
64PE332-28-3-1 m	CL	14	1	0.5	0.1	14	*0.00*			0.02	Detection limit
64PE332-28-3-20 m	CL	20	2	1	0	21	0.4	44	3	0.01	
64PE332-28-3-50 m	CL	139	14	7	3	150	2	314	25	0.01	
64PE332-28-3-93 m	CL	219	25	13	5	246	4	512	47	0.04	
64PE332-32-1-1 m	CL	16	1	1	0.2	18	0.3	36	3	0.00	
64PE332-32-1-50 m	CL	55	5	2	1	55	1	118	8	0.00	
64PE332-32-1-200 m	CL	150	22	15	4	180	6	377	47	0.00	
64PE332-32-1-500 m	CL	84	19	21	3	122	8	255	49	0.01	
64PE332-32-1-1051 m	CL	38	10	12	1	60	4	124	26	0.01	
64PE332-36-4-1 m	CL	15	1	1	0.2	17	0.3	34	2	0.00	
64PE332-36-4-50 m	CL	77	6	3	1	85	1	173	11	0.00	
64PE332-36-4-200 m	CL	41	7	6	1	53	2	111	16	0.00	
64PE332-36-4-1000 m	CL	57	16	18	2	95	7	195	43	0.00	
64PE332-36-4-2431 m	CL	19	5	5	1	30	2	63	14	0.02	
64PE332-1-1-1 m	IPL	9	1	1	*0.00*	4	*0.00*			0.26	Detection limit
64PE332-1-1-14 m	IPL	20	4	3	1.3	13	0.6	22	8	0.23	
64PE332-6-2-1 m	IPL	32	6	4	1.7	19	0.8	32	13	0.03	
64PE332-6-2-20 m	IPL	44	11	6	2.4	22	0.8	42	21	0.00	
64PE332-6-2-50 m	IPL	84	25	15	5.5	49	3.5	99	50	0.02	
64PE332-6-2-109 m	IPL	45	17	14	5.5	29	*0.00*			0.02	Detection limit
64PE332-4-2-1 m	IPL	16	2	2	0.9	10	0.7	15	5	0.01	
64PE332-4-2-50 m	IPL	85	12	8	3.5	72	2.3	97	26	0.00	

(*continued on next page*)

Appendix 5 (*continued*)

Sample name	Fraction	C1302 (μg/gOC)	C1300 (μg/gOC)	C1298 (μg/gOC)	C1296 (μg/gOC)	C1292 (μg/gOC)	C1292' (μg/gOC)	Sum of all 6 CL isoGDGTs (μg/gOC)	Sum of 4 CL isoGDGTs (μg/gOC)	BIT	Comments
64PE332-4-3-200 m	IPL	35	13	16	3.7	25	*0.00*			0.00	Detection limit
64PE332-4-2-500 m	IPL	13	5	21	1.6	15	15.8	59	44	0.00	
64PE332-4-4-1006 m	IPL	16	7	20	1.2	17	12.7	58	41	0.00	
64PE332-3-2-1 m	IPL	13	2	2	0.8	9	0.4	14	5	0.01	
64PE332-3-1-50 m	IPL	33	10	12	4.1	32	4.3	62	30	0.00	
64PE332-3-3-200 m	IPL	18	6	7	1.0	16	2.3	32	16	0.03	
64PE332-3-1-1000 m	IPL	2	1	6	0.5	4	5.7	17	13	0.00	
64PE332-3-4-1988 m	IPL	73	22	25	6.2	71	11.2	135	64	0.00	
64PE332-27-1-1 m	IPL	65	7	5	1.8	39	*0.00*			0.05	Detection limit
64PE332-27-1-19 m	IPL	35	5	5	2.0	18	1.0	31	13	0.08	
64PE332-28-3-1 m	IPL	5	1	1	0.2	3	0.2			0.05	Detection limit
64PE332-28-3-20 m	IPL	8	1	1	0.3	5	0.2	7	2	0.05	
64PE332-28-3-50 m	IPL	121	19	12	4.7	79	2.3	116	37	0.00	
64PE332-28-3-93 m	IPL	245	30	18	7.2	158	*0.00*			0.01	Detection limit
64PE332-32-1-1 m	IPL	4	1	1	0.3	3	0.2	5	2	0.17	
64PE332-32-1-50 m	IPL	30	3	2	1.2	19	0.6	26	7	0.00	
64PE332-32-1-200 m	IPL	26	6	5	1.2	25	2.3	39	14	0.00	
64PE332-32-1-500 m	IPL	23	8	19	1.4	24	13.8	66	43	0.00	
64PE332-32-1-1051 m	IPL	5	2	6	0.6	6	4.6	19	13	0.03	
64PE332-36-4-1 m	IPL	2	0.4	0.3	0.1	2	0.1	3	1	0.05	
64PE332-36-4-50 m	IPL	42	5	4	1.9	30	1.2	42	12	0.00	
64PE332-36-4-200 m	IPL	1	0.2	0.2	0.05	1	0.1	2	1	0.00	
64PE332-36-4-1000 m	IPL	31	11	21	1.7	40	13.9	88	48	0.00	
64PE332-36-4-2431 m	IPL	3	2	2	0.1	3	0.4	7	4	0.01	

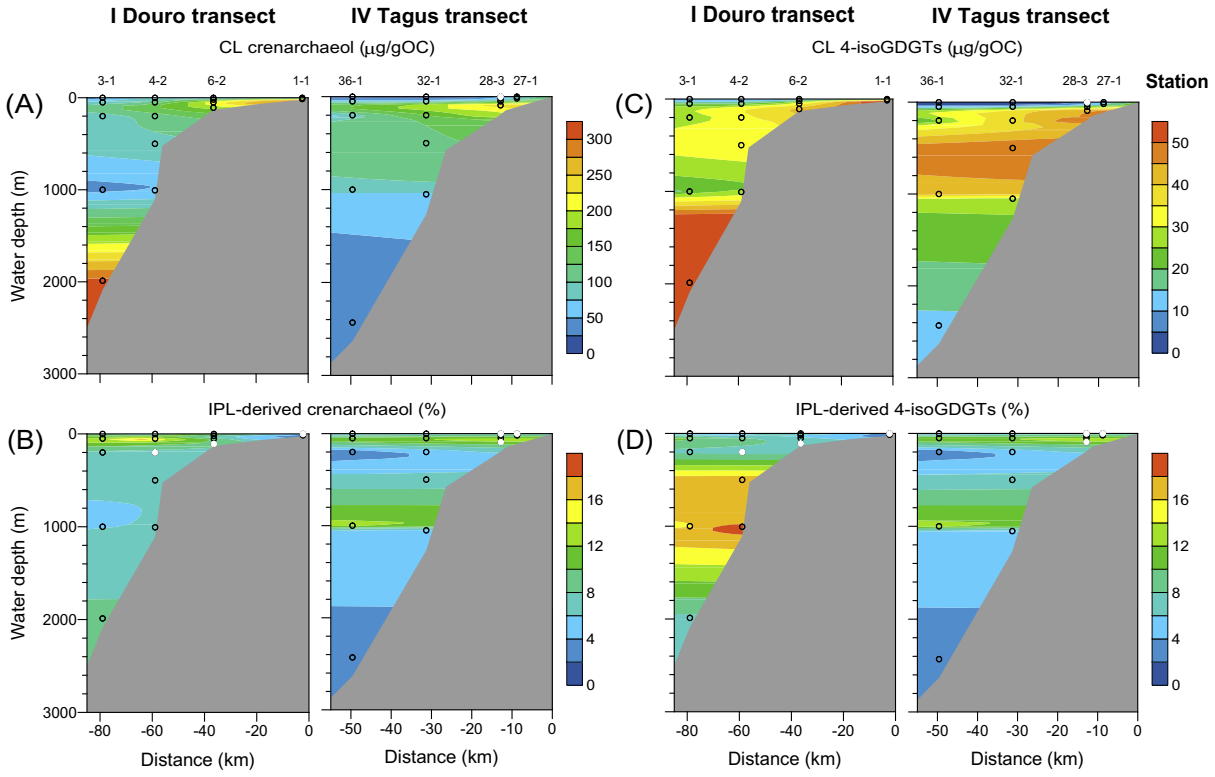

Fig. 3. Vertical distribution patterns of (A) the CL concentrations (μg/gOC), (B) the IPL-derived percentage of crenarchaeol, (C) the sum of four isoGDGTs used for the calculation of the TEX_{86}^{H}, and (D) the IPL-derived percentage of four isoGDGTs for the SPM samples collected along the Douro and Tagus transects.

4.4. Diversity, abundance and activity of Thaumarchaeota in the water column

Archaeal *amo*A and thaumarchaeotal GGGP synthase gene sequences were amplified and sequenced from SPM obtained at the Tagus transect station 36-1. DNA sequences were translated to proteins and classified into the 'shallow water' or 'deep water' cluster based on their amino acid composition and in comparison with sequences previously detected in either shallow or deep waters according to Francis et al. (2005) and Villanueva et al. (2015). Phylogenetically, most (73–100%, Fig. 7A) of the *amo*A protein sequences recovered fell in the previously defined 'Water column A/Sediment shallow water marine cluster' (Francis et al., 2005), whilst a smaller part fell in the 'Water column B deep water marine cluster'. However, there was a substantial variation with water depth. Within the first cluster, all sequences fell in tree subclusters: A.1, which also contained the *amo*A protein sequence of the marine thaumarchaeotal *Nitrosopumilus maritimus* (Appendix 8), A.3, and A.5 (Appendix 8). Sequences falling in the A.1 cluster were relatively abundant at 1 and 50 m water depth (82 and 97%, respectively; Fig. 7A); while those falling in subcluster A.5 were most abundant at 1000 m water depth (31%; Fig. 7A). The sequences falling in the 'Water column B deep water marine cluster' were most abundant at 1000 m water depth (27%; Fig. 7A). Clearly, there was a distinctive difference in the composition of *amo*A protein sequences between surface (0–50 m) and deep waters; the composition at 200 m water depth was intermediate.

Thaumarchaeotal GGGP synthases defined as the 'shallow water' type were grouped in two subclusters S.1 and S.2 (Appendix 9A), while the GGGP synthases sequences defined as the 'deep water' type recovered at 200 and 1000 m water depth were grouped in four subclusters D1 to D4 (Appendix 9B). In surface waters (SPM from 1 m and 50 m water depth) most sequences (96–100%) fell in the 'shallow water' subclusters S1 (88% and 70%, respectively) and S2 (11% and 25%, respectively) (Fig. 7B). In the deeper waters, sequences belonging to the S1 cluster were still present (18% and 34% at 200 and 1000 m water depth, respectively) but were now dominated by sequences of the 'deep water' type with the most diverse distribution (i.e. all four D-subclusters) at 1000 m water depth. As for the *amo*A protein sequences, for the thaumarchaeotal GGGP synthases, we observed a clear difference between shallow (0−50 m) and deep (1000 m) water SPM but, in contrast, the SPM from 200 m water depth was more like the deep water.

Thaumarchaeotal 16S rRNA gene copy number ranged from 1.4×10^3 to 5.7×10^5 gene copies L^{-1} with lowest values at 200 m water depth and highest at 50 m water depth. Archaeal *amo*A gene copies per liter were highest at 50 m water depth (4.4×10^5 *amo*A gene copies L^{-1}), and lowest at 200 m water depth (7.5×10^2 *amo*A gene copies L^{-1}) (Fig. 8A). At 1000 m water depth, the abundance of

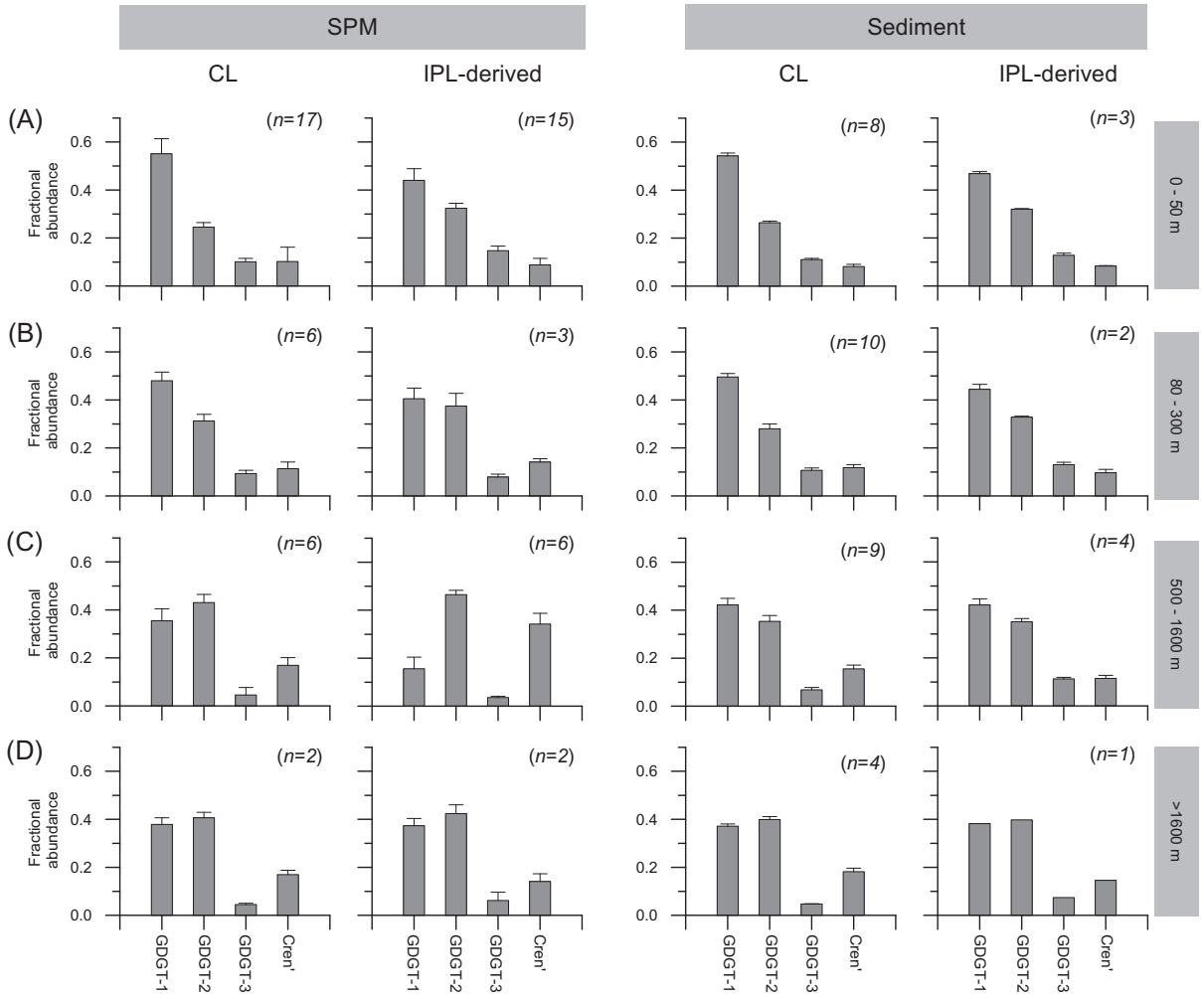

Fig. 4. Average fractional abundance of CL and IPL-derived isoGDGT used for TEX_{86}^{H} in SPM and surface sediments collected at stations located at a water depth of (A) 0 m and 50 m (surface mixed layer), (B) 80 m and 300 m, (C) 500 m and 1600 m (MOW), and (D) >1600 m.

archaeal *amo*A gene copies increased up to 1.5×10^4 *amo*A gene copies L^{-1} (Fig. 8A). The ratio of *amo*A mRNA transcripts to *amo*A gene copies (RNA:DNA ratio) could only be estimated at 50 m and 200 m water depth (0.008 and 0.6, respectively) as *amo*A gene transcripts could not be detected at 1 m and 1000 m water depth (Fig. 8A).

5. DISCUSSION

5.1. Vertical distribution of isoGDGTs in the water column and its relation to thaumarchaeotal populations

The BIT index of all marine SPM samples (Zell et al., 2014, 2015) was relatively low with values ranging from 0 to 0.26 for both CL and IPL-derived GDGTs (Fig. 9A; see also Appendix 5). The higher BIT values (0.16 ± 0.08) were found closest to the coast at shallow water depth (<20 m), whilst those from deeper waters were low (0.01 ± 0.03). Overall, the BIT index of marine SPM was much lower than that of the Tagus River SPM collected close to the river mouth (0.71 ± 0.08 and 0.56 ± 0.13 for CL and IPL-derived fractions, respectively; Zell et al., 2014). Furthermore, most of the BIT values in marine SPM were well below the cut-off value (0.3) proposed earlier (Weijers et al., 2006). This suggests that continental-derived, i.e. soil- and/or river-derived (cf. Hopmans et al., 2004; Zell et al., 2013a,b; De Jonge et al., 2014) organic matter input, as reflected in the BIT index, does not influence the distribution of isoGDGTs in SPM along the Portuguese continental margin to a significant extent.

The vertical concentration profiles of CL isoGDGTs were, to some extent, different along the Douro and Tagus transects (Fig. 3A and C). In general, the CL isoGDGT concentrations were higher in the bottom water layers on the shelf. This might be associated with sediment resuspension from the seabed, considering the enhanced turbidity in the bottom water layer on the shelf (Appendix 4). Our results are in a good agreement with the previous observations of sediment resuspension induced by nonlinear internal waves over the Portuguese continental shelf (e.g. Quaresma et al., 2007). Notably, the SPM sample collected at 1988 m water depth at station 3-1 in the Douro transect has the highest concentration of CL isoGDGTs. This might also be related to sediment resuspension, probably caused

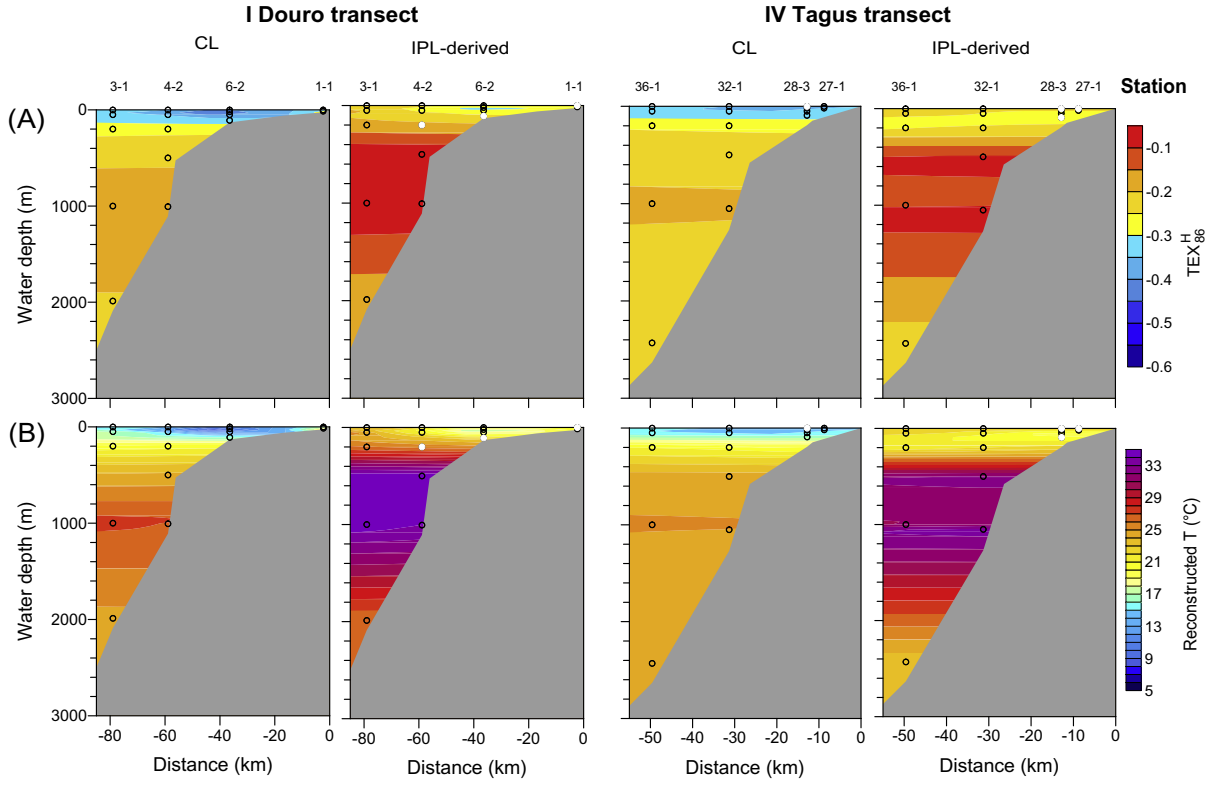

Fig. 5. Vertical distribution patterns of (A) TEX_{86}^{H} and (B) TEX_{86}^{H}-derived SSTs for the SPM samples collected along the Douro and Tagus transects.

by contact of the CTD frame with the sea floor during the sampling. However, the resuspended organic-rich material has only a little effect on the distribution of isoGDGTs and thus the TEX_{86}^{H} signal in SPM since most distinctive changes are observed outside the zone of sediment resuspension (see the discussion below).

The CL concentrations of four isoGDGTs used for the TEX_{86}^{H} were higher at water depths >100 m at the offshore sites, i.e. below the upper layer of the water column where the primary productivity takes place (Fig. 3C, see also Appendix 4). IPL-derived isoGDGT concentrations and %IPL values of these four isoGDGTs were higher at 500–1600 m along the Douro and Tagus transects (Fig. 3D). Interestingly, this water mass corresponds to the MOW, characterized by warm, saline, and depleted oxygen conditions (Fig. 2). The MOW water mass is also characterized by higher TEX_{86}^{H} values and thus warmer TEX_{86}^{H}-derived temperatures for both CL and IPL-derived fractions, although the "warm signature" is much more evident for the IPL-derived fractions (Fig. 5). The distinct difference in distribution of IPL-derived isoGDGTs between the surface mixed layer (0–50 m water depth) and the MOW is especially evident from the higher fractional abundance of crenarchaeol regio-isomer and the lower fractional abundance of GDGT-1 (Fig. 4C). The distribution of CL isoGDGTs shows that the elevated CL TEX_{86}^{H} values in the MOW co-occur with an increase in fractional abundances of GDGT-2 and crenarchaeol regio-isomer but a decrease of the fractional abundance of GDGT-1 and GDGT-3, in comparison to those in the surface mixed layer (Figs. 5A, C, and 9).

A recent study in the Mediterranean Sea (Kim et al., 2015) showed that the fractional abundances of GDGT-2 and the crenarchaeol regio-isomer were much higher in the CL fractions of deep-water SPM than in the shallow-water SPM, while GDGT-1 and GDGT-3 displayed an opposite trend. This is similar to what we observe for the Portuguese margin (Fig. 10). It has been postulated that the isoGDGT distribution in deeper waters might be different from that in shallow waters due to the presence of a different thaumarchaeotal community in the Mediterranean Sea (Kim et al., 2015). Interestingly, the IPL-derived isoGDGT distribution in deeper waters along the Portuguese margin closely mimics the CL isoGDGT distribution in deeper waters in the Mediterranean Sea, although fractional abundances of IPL-derived crenarchaeol regio-isomer are even higher in the Portuguese margin (Fig. 10). This suggests that a similar 'deep water' thaumarchaeotal community might thrive in the MOW along the Portuguese margin, producing isoGDGTs with a different distribution in deeper waters in comparison to those in shallow waters. Notably, elevated CL TEX_{86}^{H} values, due to increases in fractional abundances of GDGT-2 and crenarchaeol regio-isomer, have also been observed in the oxygen minimum zones (OMZs) of the Arabian Sea (Schouten et al., 2012) and off Cape Blanc, NW Africa (Basse et al., 2014). Previous studies have suggested that oxygen deficiency or combined factors such as low oxygen, high water

Appendix 6
Concentrations of CL and IPL-derived isoGDGTs normalized to OC and BIT values for marine surface sediments obtained by both BD and ASE extractions.

Sample name	Fraction	Extraction technique	C1302 (μg/gOC)	C1300 (μg/gOC)	C1298 (μg/gOC)	C1296 (μg/gOC)	C1292 (μg/gOC)	C1292' (μg/gOC)	Sum of all 6 CL isoGDGTs (μg/gOC)	Sum of 4 CL isoGDGTs (μg/gOC)	BIT
I. Douro transect											
64PE332-1-3	CL	ASE	198	21	9	4	175	3	410	36	0.12
64PE332-7-2	CL	ASE	486	49	25	11	465	8	1043	93	0.06
64PE332-7-2	CL	BD	297	31	15	7	301	5	656	58	0.05
64PE332-7-2	IPL	BD	25	4	3	1	15	1	48	8	0.11
64PE332-9-1	CL	ASE	243	34	19	8	364	7	675	68	0.03
64PE332-6-1	CL	ASE	285	38	20	8	309	10	670	76	0.04
64PE332-6-1	CL	BD	153	20	11	4	174	4	366	39	0.04
64PE332-6-1	IPL	BD	10	2	2	1	7	1	22	5	0.13
64PE332-5-2	CL	ASE	307	52	36	9	364	16	784	113	0.02
64PE332-5-2	CL	BD	118	22	15	4	149	0.2	308	41	0.01
64PE332-5-2	IPL	BD	11	3	2	1	11	1	28	6	0.03
64PE332-4-1	CL	ASE	163	33	30	5	230	13	473	81	0.02
64PE332-4-1	CL	BD	43	9	8	1	61	3	125	21	0.02
64PE332-4-1	IPL	BD	4	1	1	0.2	4	0.3	10	2	0.03
64PE332-3-7	CL	ASE	197	44	48	5	285	19	599	116	0.01
64PE332-3-7	CL	BD	92	21	23	3	136	9	284	56	0.01
64PE332-3-7	IPL	BD	8	1	2	0.3	7	1	19	4	0.01
II. Mondego transect											
64PE332-11-2	CL	ASE	488	49	23	10	454	7	1030	88	0.05
64PE332-12-1	CL	ASE	596	89	47	20	898	16	1667	172	0.02
64PE332-13-3	CL	ASE	513	101	78	17	715	31	1455	227	0.01
64PE332-14-4	CL	ASE	141	33	33	5	230	15	457	85	0.01
64PE332-15-1	CL	ASE	278	65	71	8	426	30	880	175	0.01
III. Estremadura transect											
64PE332-24-2	CL	ASE	656	85	42	17	694	11	1505	155	0.02
64PE332-17-2	CL	ASE	700	91	44	19	733	12	1599	166	0.03
64PE332-18-5	CL	ASE	444	65	36	15	565	17	1142	132	0.02
64PE332-25-2	CL	ASE	457	67	35	14	562	19	1155	135	0.02
64PE332-26-2	CL	ASE	993	169	110	33	1251	40	2597	353	0.01
64PE332-20-2	CL	ASE	291	53	37	10	404	15	811	115	0.01
64PE332-22-6	CL	ASE	211	50	51	7	322	20	662	129	0.01
64PE332-23-2	CL	ASE	206	46	51	6	309	25	643	128	0.01

(*continued on next page*)

Appendix 6 (*continued*)

Sample name	Fraction	Extraction technique	C1302 (μg/gOC)	C1300 (μg/gOC)	C1298 (μg/gOC)	C1296 (μg/gOC)	C1292 (μg/gOC)	C1292' (μg/gOC)	Sum of all 6 CL isoGDGTs (μg/gOC)	Sum of 4 CL isoGDGTs (μg/gOC)	BIT
IV. Tagus transect											
64PE332-27-3	CL	ASE	181	18	9	4	168	3	382	34	0.15
64PE332-27-3	CL	BD	344	36	18	7	349	5	758	66	0.16
64PE332-27-3	IPL	BD	80	11	7	3	43	2	146	22	0.17
64PE332-29-2	CL	ASE	364	39	19	8	373	6	809	72	0.07
64PE332-29-2	CL	BD	92	10	5	2	95	1	205	18	0.08
64PE332-29-2	IPL	BD	15	3	2	1	10	0.4	30	5	0.11
64PE332-30-1	CL	ASE	271	35	19	8	325	8	666	70	0.05
64PE332-28-1	CL	ASE	150	17	9	4	171	4	355	34	0.07
64PE332-28-1	CL	BD	151	17	9	4	175	3	359	33	0.07
64PE332-28-1	IPL	BD	19	4	3	1	11	1	38	8	0.15
64PE332-31-2	CL	ASE	370	64	47	12	505	20	1018	143	0.02
64PE332-31-2	CL	BD	19	3	2	1	26	1	52	7	0.02
64PE332-31-2	IPL	BD	2	0.4	0.4	0.1	1	0.1	4	1	0.05
64PE332-33-1	CL	ASE	277	58	49	9	403	24	819	140	0.02
64PE332-33-1	CL	BD	28	6	5	1	41	2	82	14	0.02
64PE332-33-1	IPL	BD	3	1	1	0.2	3	0.3	8	2	0.04
64PE332-36-3	CL	ASE	177	38	38	5	269	20	547	102	0.03
V. Sado transect											
64PE332-34-2	CL	ASE	120	15	8	3	151	3	300	29	0.08
64PE332-38-2	CL	ASE	444	59	34	13	523	13	1085	119	0.04
64PE332-37-2	CL	ASE	244	41	30	7	326	13	662	92	0.02
64PE332-40-1	CL	ASE	249	52	47	8	367	23	746	130	0.02

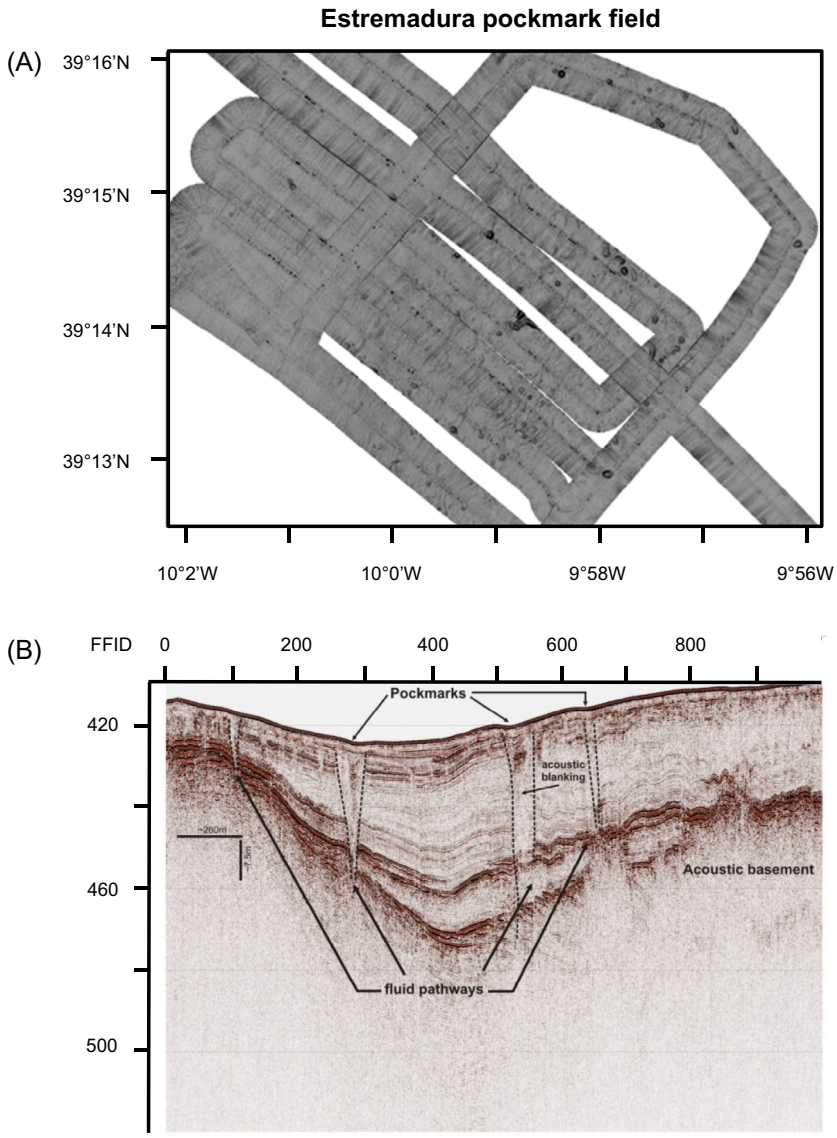

Appendix 7. Multibeam (A) and seismic (B) data from the pockmarks area discovered in the Estremadura Spur. Initially, a ~100 m wide pockmarks was unexpectedly discovered at ~300 m water depth during the multibeam and seismic survey in the Estremadura Spur. The analysis of the data allowed the observation of more than 30 pockmarks. Some pockmarks are partially filled with sediments along the fluid circulation pathways that appear to reach the acoustic basement of the Mesozoic age.

pressure, and nutrient limitation are possible environmental factors determining the segregation of 'shallow water' and 'deep water' Thaumarchaeota, which might produce isoGDGTs with a different distribution (e.g. Basse et al., 2014; Villanueva et al., 2015). The IPL-derived isoGDGTs in the MOW along the Portuguese margin show a distribution that is comparable to those in the OMZ in the Arabian Sea (Fig. 10). Hence, by analogy with the OMZ, it might be probable that the MOW hosts a different thaumarchaeotal community due to the oxygen-deficiency (see Fig. 2). This thaumarchaeotal population present in the MOW would produce isoGDGTs with a higher fractional abundance of GDGT-2 and crenarchaeol regio-isomer and a lower fractional abundance of GDGT-1 and GDGT-3, resulting in the elevated TEX_{86}^{H} values detected in our study. However, the reduction of the oxygen concentration in the MOW is only ~30%, much less than in the OMZ. Therefore, it is likely that changes in isoGDGT distribution might also depend on other environmental factors than oxygen concentration.

To test the hypothesis of different thaumarchaeotal populations in the MOW, we performed phylogenetic analysis of the thaumarchaeotal genes coding for *amo*A and GGGP synthase proteins at Tagus station 36-1 at four different depths. These results clearly indicated the division of 'shallow water' and 'deep water' thaumarchaeotal communities based on the GGGP synthase (Fig. 7B) and somewhat more subtle differences based on *amo*A (Fig. 7A). These large changes are consistent with the marked change observed in IPL-derived and, to a lesser extent, CL isoGDGTs with

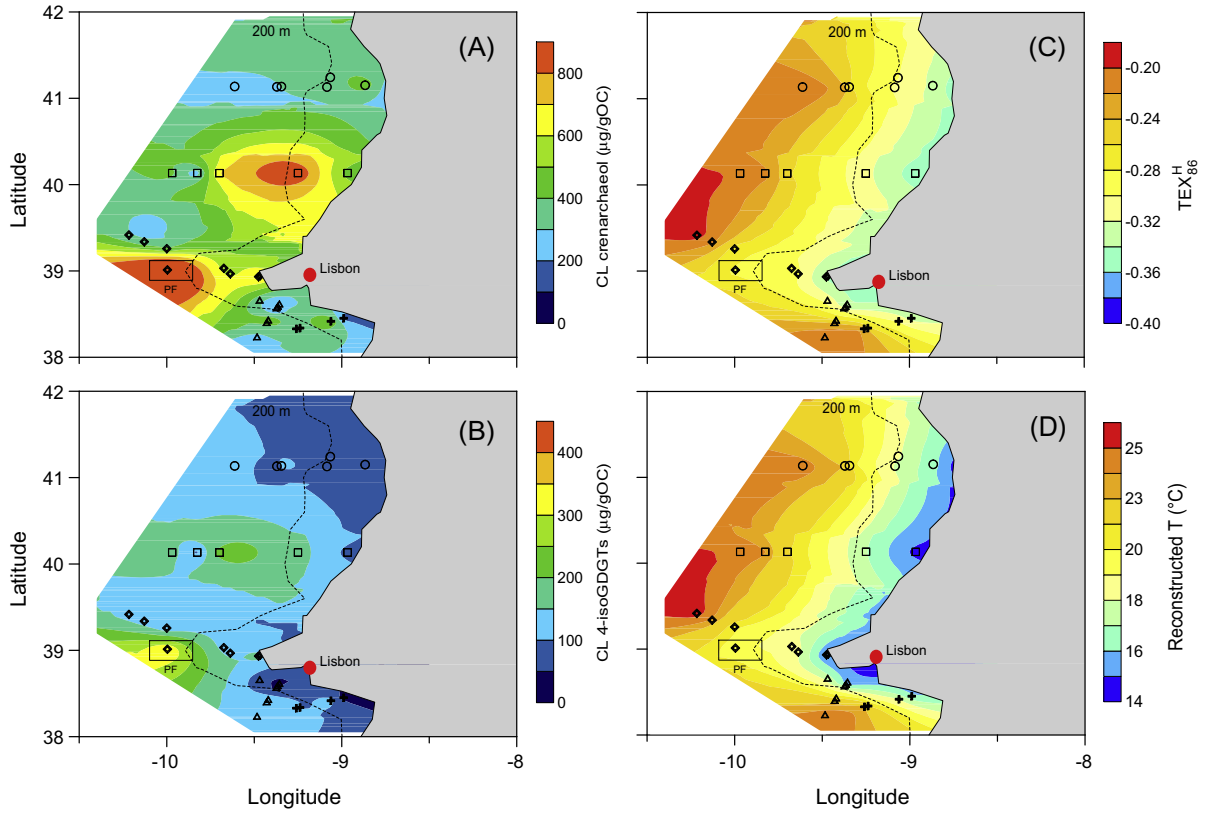

Fig. 6. Spatial distribution patterns of the CL concentrations (µg/gOC) of (A) crenarchaeol and (B) the sum of four isoGDGTs used for the calculation of the TEX_{86}^{H}, (C) TEX_{86}^{H}, and (D) TEX_{86}^{H}-derived SSTs for the surface sediments. The 200 m isobath line is indicated for reference as a dashed line. PF indicates "pockmark field".

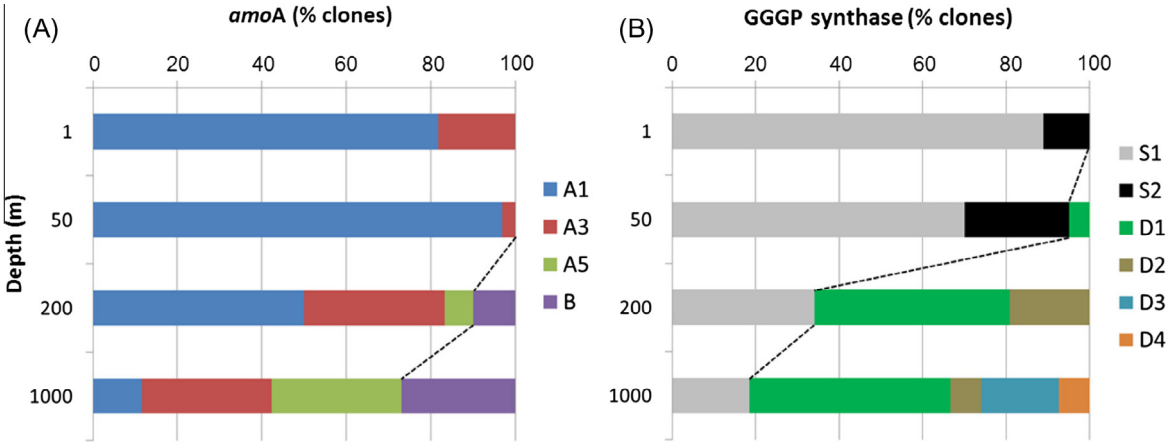

Fig. 7. Relative contribution (as % of clones) of archaeal ammonia monoxygenase (*amo*A) (A) and thaumarchaeotal GGGP synthase protein sequences (B) of the different 'shallow' and 'deep water' subclusters defined in Fig. 18, in the SPM of the Tagus transect station 36-1. The stippled line depicts the separation between 'shallow' and 'deep water' sequences.

increasing water depth (Figs. 4 and 5). This is also in good agreement with Villanueva et al. (2015), who also coupled the changes in distribution of isoGDGTs with increasing water depth to distinct changes in the thaumarchaeotal population, which can, in general, be subdivided into 'shallow water' and 'deep water' types. Importantly, however, the lack of detectable *amo*A gene transcripts at 1000 m (Fig. 8A) suggests a much-reduced activity based on oxidation of ammonia of the Thaumarchaeota population in the MOW, or alternatively a metabolism independent of ammonia (e.g. Qin et al., 2014). Such a low activity of Thaumarchaeota in deep waters has previously been observed in other settings (Santoro et al., 2010; Pitcher et al., 2011) and actually raises the question whether the

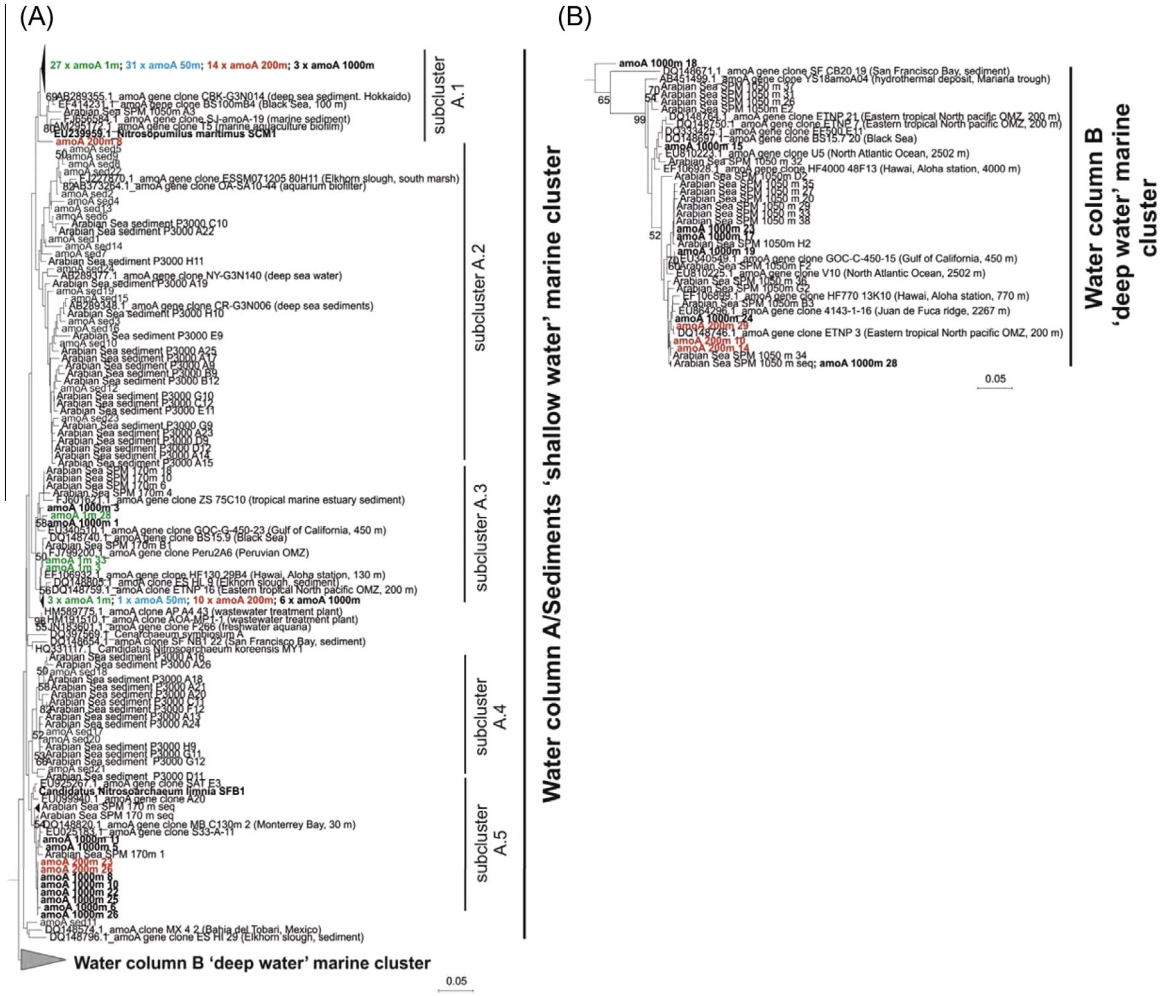

Appendix 8. Neighbor-joining tree of *amo*A protein sequences recovered from SPM samples of the Tagus transect station 36-1 at 1 m (green), 50 m (blue), 200 m (red), 1000 m (black), constructed with the Neighbor-Joining method (Saitou and Nei, 1987). Scale bar indicates 5% sequence dissimilarity. (A) Clusters of Water column A/Sediments ('shallow water' marine clade) and Water column B ('deep water' marine clade) of the *amo*A gene were defined by Francis et al. (2005). (B) The expansion of the cluster B 'deep water' marine clade. The evolutionary distances were computed using the Poisson correction method with a bootstrap test of 1000 replicates (values higher than 50% are shown on the branches). *Amo*A sequences amplified from 170 and 1050 m SPM in the Arabian Sea and surface sediment at 3003 m water depth (P3000) by Villanueva et al. (2015) are also included in the tree for comparison. Subclusters are defined in the text. Sequences recovered from the surface sediment underneath the SPM sampling location (1989 m water depth) are also indicated in the tree as 'amoA sed'. (For interpretation of the references to colour in this figure legend, the reader is referred to the web version of this article.)

detected genetic (and isoGDGT) signatures are derived from a thriving population of Thaumarchaeota or reflect transportation of cells from another location. Since the MOW is sourced by Mediterranean deep water, which is characterized by this characteristic isoGDGT pattern (Fig. 10), transportation of cells is a plausible explanation. Comparison of the thaumarchaeotal gene composition of Mediterranean deep water with that of the MOW is required to confirm this hypothesis.

5.2. Impact of the presence of thaumarchaeotal deep water populations on the spatial distribution of isoGDGTs in surface sediments

The CL BIT values of the surface sediments (0.01–0.15; Zell et al., 2015) were, in general, substantially lower than those of the Tagus River SPM collected close to the river mouth (0.71 ± 0.08; Zell et al., 2014). The highest CL BIT values were found close to the coast (at £20 m water depth) and rapidly decreased with increasing water depth towards the open ocean sites (Fig. 9A). As observed for marine SPM, most of the CL BIT values in core-top sediments were well below the cut-off value (0.3) for application of the TEX_{86} palaeothermometer proposed earlier (Weijers et al., 2006). This indicates that the input of continental organic matter affects the distribution of isoGDGTs in surface sediments along the Portuguese continental margin only to a minor extent.

The CL TEX_{86}^{H} values and derived SSTs in the surface sediments were lower along the coast and gradually increased towards offshore sites (Fig. 6C and D). The CL TEX_{86}^{H} values and the derived SSTs indeed reveal a strong

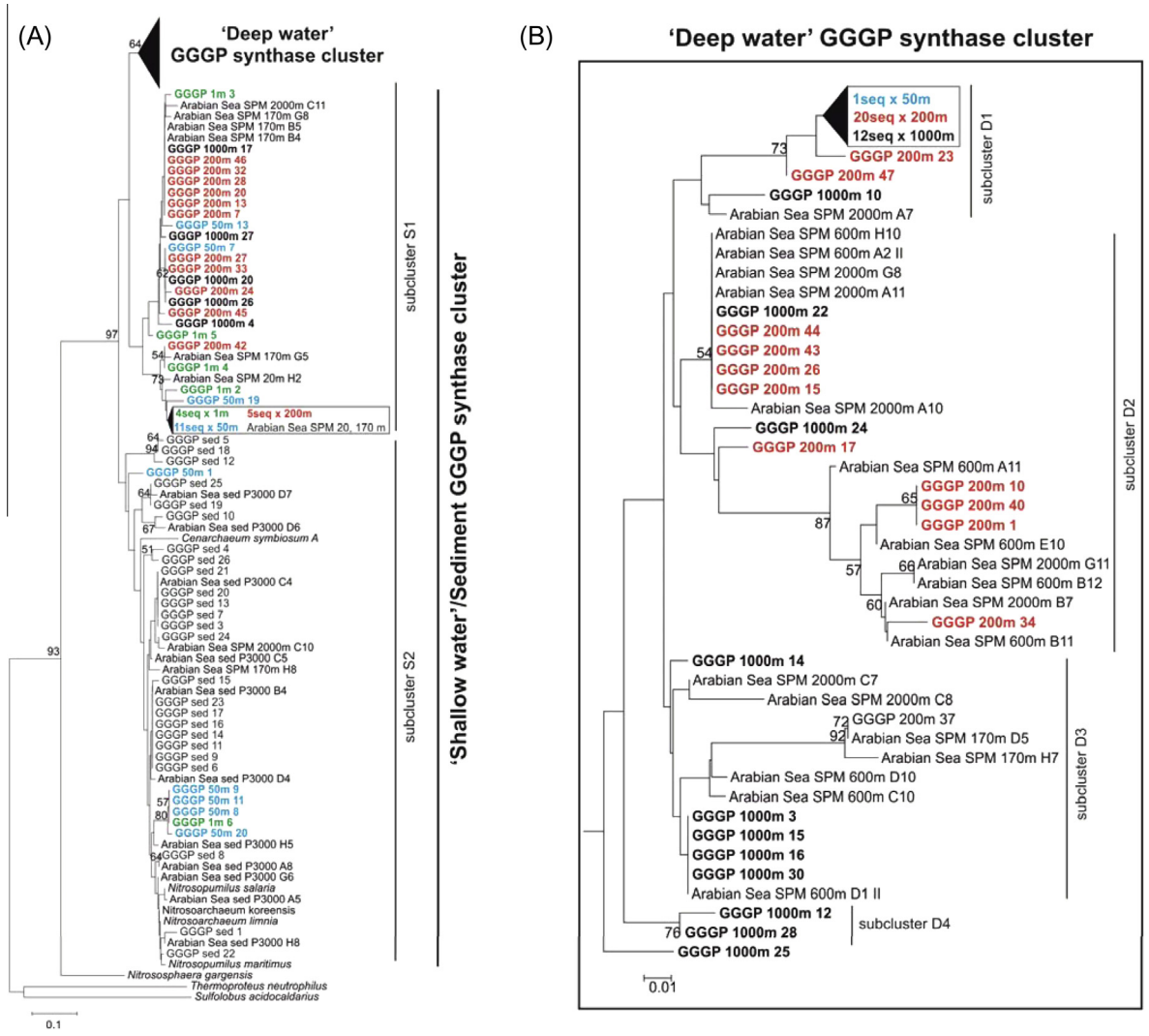

Appendix 9. (A) Phylogenetic tree of putative partial GGGP synthases recovered from the Tagus transect station 36-1 SPM at 1 m, 50 m, 200 m, and 1000 m water depth, revealing 'shallow' and 'deep water' GGGP synthases clusters. The analysis involved 140 amino acid sequences with 78 amino acid residues. The phylogenetic tree was inferred by neighbor-joining with the Poisson correction method. Branch support was calculated with a bootstrap tree of 1000 replicates (values higher than 50% are indicated on the branches). The scale bar indicates evolutionary distance of 0.1 substitutions per site. (B) The expanded subtree of the 'deep water' GGGP synthase cluster. Sequences recovered from the surface sediment underneath the SPM sampling location (1989 m water depth) are also indicated in the tree as 'GGGP sed'. (For interpretation of the references to colour in this figure legend, the reader is referred to the web version of this article.)

positive trend versus water depth ($r^2 = 0.97$, black line; Fig. 9B and C), while the correlation of satellite-derived annual mean SST with water depth is substantially weaker ($r^2 = 0.51$, black line; Fig. 9D) and hardly shows a trend. With increasing water depth, the fractional abundances of GDGT-2 and crenarchaeol regio-isomer increased while those of GDGT-1 and GDGT-3 decreased (black lines, Fig. 9E), resulting in the observed trend in TEX_{86}^{H}. Hence, it appears that the sedimentary distribution of CL isoGDGTs used in TEX_{86}^{H} along the Portuguese margin is primarily influenced by water depth. This special distribution pattern is thus identical to the observed pattern in the Ligurian Sea (Kaiser et al., 2014), the Gulf of Lions, the Gulf of Taranto, and the Balearic Sea (Kim et al., 2015), all part of the Mediterranean Sea. Indeed, when the data from surface sediments in the Mediterranean Sea are plotted (red line; Fig. 9B–E; Kim et al., 2015) together with those from the Portuguese Margin, they show a remarkably similar trend.

The water depth trend observed in the distribution of isoGDGTs in the CL fractions of the surface sediments was similar to that observed in the SPM for both IPL-derived and, to a lesser extent, CL isoGDGTs, i.e. increased fractional abundance of GDGT-2 and the crenarchaeol regio-isomer in deep water (blue filled squares; Fig. 9B and C, E). The different isoGDGT distribution in SPM in deeper waters from that in surface waters is proposed to be due to the presence of a different thaumarchaeotal community in deeper waters (see Section 5.1). In particular the IPL-derived isoGDGTs of the SPM from the MOW layer along the Portuguese Margin show a higher fractional abundance of the crenarchaeol regio-isomer but a

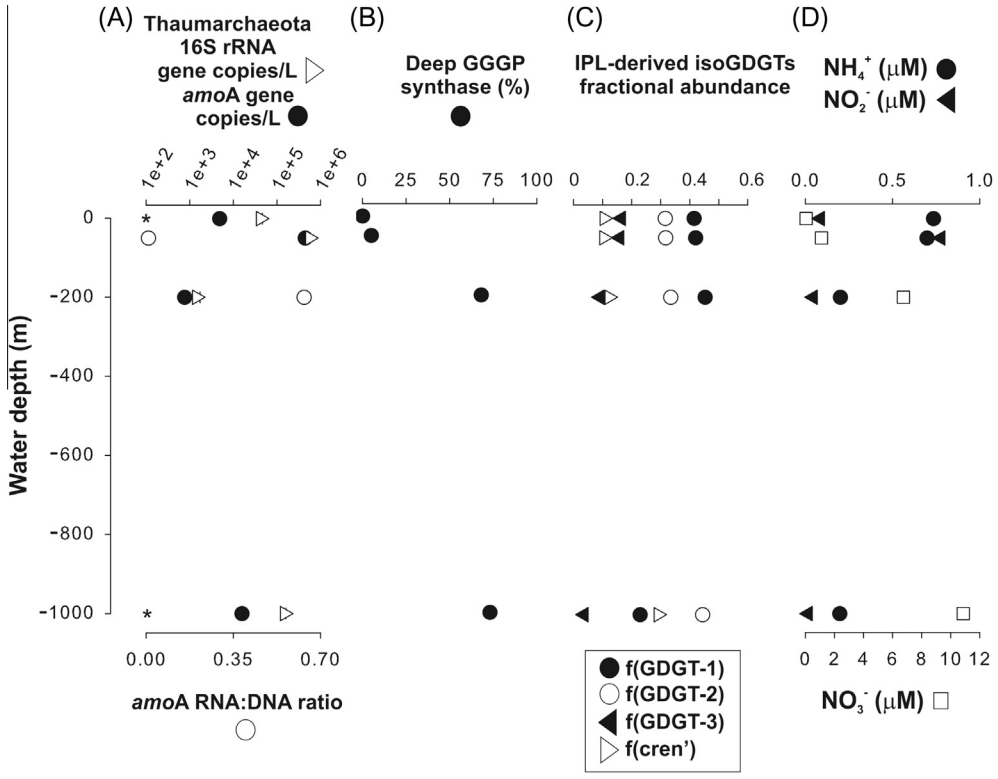

Fig. 8. Comparison of molecular ecological data with isoGDGT distributions and nutrient profiles for the Tagus transect station 36-1. (A) Thaumarchaeotal 16S rRNA gene abundance, archaeal ammonia monoxygenase (*amo*A) gene abundance, and *amo*A RNA:DNA ratio, (B) percentage of 'deep water' thaumarchaeotal GGGP synthase, (C) fractional abundances of IPL-derived isoGDGTs, and (D) concentration of selected nutrients. Asterisks indicate below detection limit.

lower fractional abundance of GDGT-1 in comparison to those in the surface mixed layer (purple filled square; Fig. 9E), leading to higher TEX_{86}^{H} values and higher reconstructed temperatures (purple filled square; Fig. 9B and C). Taken together, our SPM and surface sediment data suggest that with increasing water depth, the deep-water population of Thaumarchaeota residing in the MOW contributes increasingly to the pool of sedimentary isoGDGTs, thereby influencing the TEX_{86}^{H} values.

To estimate the potential effect of the deep-water dwelling Thaumarchaeota in the MOW on the surface sedimentary distribution of isoGDGTs, we calculated the proportions of deep-water derived isoGDGTs relative to the total CL isoGDGTs in surface sediments, using a simple two end-member mixing model. As the end-member of the surface mixed layer, we used the average distribution of CL isoGDGTs in SPM collected between 0 m and 50 m water depth (Fig. 5A). As the deep-water (MOW) end-member, the average IPL-derived isoGDGT distribution of SPM collected between 500 m and 1600 m water depth (Fig. 4C) was used. The two end-member mixing model is defined as follows:

$$f_{dw} = \frac{(X_{ss} - X_{sm})}{(X_{dw} - X_{sm})} * 100\% \quad (4)$$

where f_{dw} is the deep-water isoGDGT proportion, X_{ss} is the fractional abundance of the isoGDGTs in the surface sediments, and X_{sm} and X_{dw} are the end-member values of the surface mixed layer and the deep-water (MOW) layer, respectively. We used the summed fractional abundances of GDGT-2 and the crenarchaeol regio-isomer for X since both showed an increasing trend with water depth (Fig. 9). Consequently, $X_{sm} = 0.35$ and $X_{dw} = 0.81$. Using this model, the estimated proportion of the deep-water derived isoGDGTs in the surface sediments reached up to 54% and showed a consistent increase with increasing water depth (Fig. 11). Due to this trend, the TEX_{86}^{H}-derived SSTs of up to 27 °C in the surface sediments substantially deviate from the surface water end-member value of 15 °C. This difference of up to 12 °C is substantially larger than the error range of the TEX_{86}^{H} temperature estimates, i.e. ±3 °C, which includes the uncertainty associated with the calibration (±2.5 °C; Kim et al., 2010a) and the analytical error (0.2 °C).

The strong influence of 'deep water' Thaumarchaeota on sedimentary isoGDGT distributions as observed here, and, thus, a strong control of water depth on the TEX_{86}^{H} paleothermometry is not in line with many earlier studies. For example, in the North Atlantic off Cape Blanc (Africa), elevated CL and IPL TEX_{86}^{H} values were observed in SPM from deeper waters in the OMZ (see the Section 5.1), but this did not affect the sedimentary CL TEX_{86}^{H} signal (Basse et al., 2014). Similarly, previous studies in the anoxic Black Sea and Cariaco Basin have shown that CL TEX_{86}^{H} values in sinking particles and surface sediments reflect

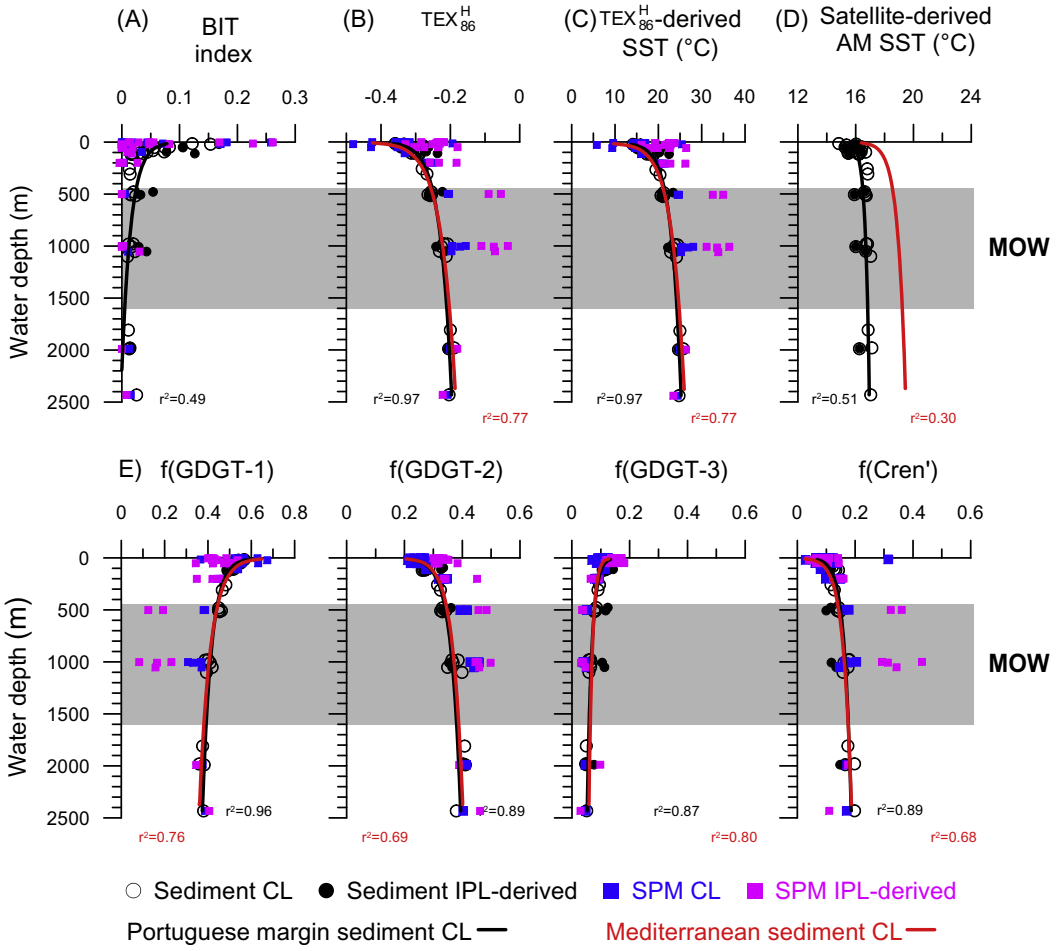

Fig. 9. Vertical water depth profiles of (A) the BIT values from Zell et al. (2014, 2015), (B) TEX^H_{86}, (C) TEX^H_{86}-derived SSTs, (D) satellite-derived annual mean SSTs (based on data from Casey and Cornillon, 1999), and (E) fractional abundances of four isoGDGTs used to calculate the TEX^H_{86} a. Logarithmic regression lines are plotted for the Portuguese margin data set (black line) in comparison to the Mediterranean data set (Kim et al., 2015; red line). Determination coefficient (r^2) values are given. The SPM data were not used for the regression of the data. (For interpretation of the references to color in this figure legend, the reader is referred to the web version of this article.)

conditions in the near-surface oxic layer (Wakeham et al., 2003; Turich et al., 2013). A lack of transport mechanism such as aggregates or fecal pellets capable of sinking and incorporating isoGDGTs formed at deeper water depth has been invoked for its explanation (e.g. Wuchter et al., 2005; Huguet et al., 2006). An important question arising from our work is, thus, why we do observe the effect of deep-water derived isoGDGTs in the surface sediments along the Portuguese continental margin and in the Mediterranean Sea? And secondly, how common is this on a global scale? The reason for the difference between the Mediterranean Sea/the Portuguese continental margin and other oxygen-depleted basins remains to be fully understood. Nonetheless, it is noteworthy that the bottom water of the Mediterranean Sea and the MOW along the Portuguese continental margin are characterized by more warm, saline, and denser waters than in other basins. This leads us to speculate that such environmental conditions might be favorable for the deep-water produced isoGDGT preservation and/or transport from the water column to the seafloor although we fail to understand the mechanisms involved. Clearly, this is an important issue to be addressed for the application of the TEX^H_{86} paleothermometry in down core studies.

Intriguingly, the highest concentration of four CL isoGDGTs used in TEX^H_{86} is found in the pockmarks field (Fig. 6A and B). Seabed pockmarks are fluid/gas escape chimneys, which appear as cone-shaped circular or elliptical depressions (e.g. Hovland and Judd, 1988) and which are often associated with gas hydrate bearing sediments in continental margin settings worldwide (e.g. Hovland et al., 2005). Therefore, it would be expected that the sedimentary distribution of isoGDGTs in the pockmarks field is influenced by the anaerobic methane-oxidizing archaea synthesizing isoGDGTs (e.g. Pancost et al., 2001; Blumenberg et al., 2004), causing an increase in TEX^H_{86} values (e.g. Weijers et al., 2011b). However, the sedimentary distribution of CL isoGDGTs in the pockmarks field is similar to that of other shelf sediments. Furthermore, the highest TEX^H_{86} value is observed in the open ocean sites rather than

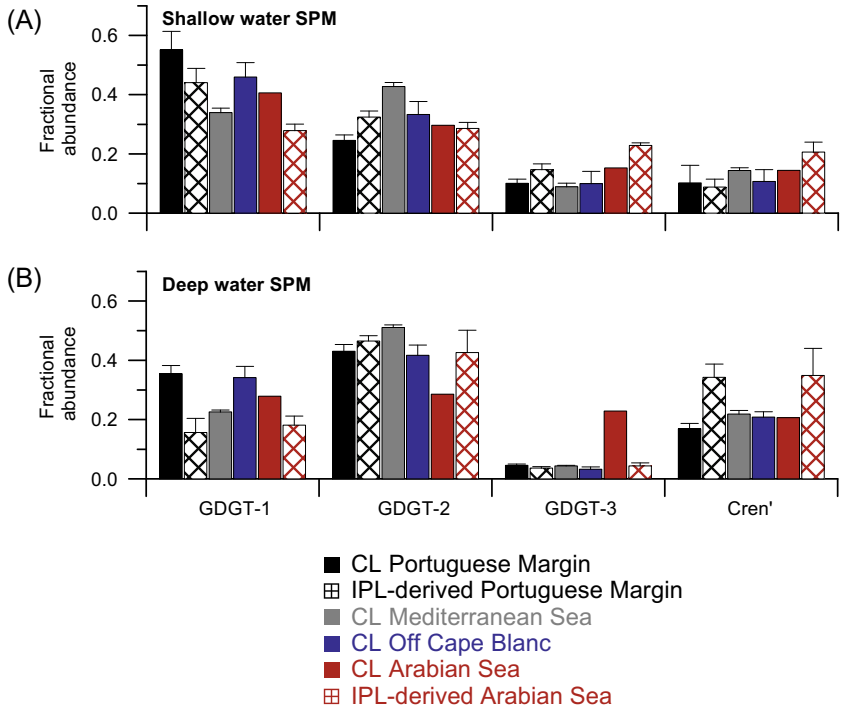

Fig. 10. Comparison of the average distribution of the four isoGDGTs used for the TEX_{86}^{H} between (A) shallow (0–50 m water depth) water SPM collected from the Portuguese margin, the Mediterranean Sea (Kim et al., 2015), off Cape Blanc (NW Africa, Basse et al., 2014), and the Arabian sea (Schouten et al., 2012) and (B) deep water SPM taken from the MOW along the Portuguese margin, the Mediterranean Sea (Kim et al., 2015), and the OMZ off Cape Blanc (NW Africa, Basse et al., 2014) and the Arabian Sea (Schouten et al., 2012).

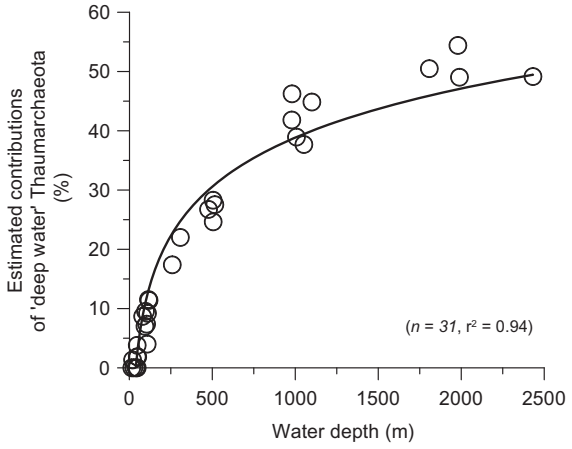

Fig. 11. Percentages of deep-water derived isoGDGTs obtained from a simple binary mixing model versus water depth. A logarithmic regression line is fitted through the data (black line).

in the pockmarks field (see Fig. 6). Accordingly, it appears that water depth is the major environmental factor influencing the sedimentary distribution of isoGDGTs along the Portuguese continental margin.

6. CONCLUSIONS

We investigated whether the distributions of isoGDGTs along the Portuguese continental margin might be influenced by the warm and saline, oxygen-depleted MOW by analysing SPM and surface sediments. We compared the concentration and distribution of IPL-derived isoGDGTs in SPM with the diversity, abundance, and activity of Thaumarchaeota based on the genetic analysis of the genes coding for the *amo*A and the GGGP synthase involved in the isoGDGT biosynthetic pathway. Higher TEX_{86}^{H} values and thus warmer TEX_{86}^{H}-derived temperatures were obtained from the deep-water SPM collected from the MOW layer for both CL and IPL-derived fractions. GDGT-2 and the crenarchaeol regio-isomer were more dominant in the deep-water SPM than in the shallow-water SPM while GDGT-1 and GDGT-3 displayed an opposite trend. Phylogenetic analyses based on the archaeal *amo*A and the GGGP synthase proteins revealed that Thaumarchaeota populations detected at 1 m and 50 m water depth were different from those detected in 200 m and 1000 m water depth, which had an increasing contribution of 'deep water' Thaumarchaeota. The CL TEX_{86}^{H} in the surface sediments also revealed a strong positive trend versus water depth. The increasing CL TEX_{86}^{H} trend is accompanied by increasing fractional abundances of CL GDGT-2 and CL crenarchaeol regio-isomer and decreasing fractional abundances of CL GDGT-1 and CL GDGT-3 with water depth. These differences in the fractional abundances of isoGDGTs with water depth are compatible with the increasing contribution of 'deep water' Thaumarchaeota harboring a different GGGP synthase enzyme. Accordingly, using integrated lipid and nucleic acid analyses, we show that with increasing water depth, the deep-water

population of Thaumarchaeota residing in the MOW contribute increasingly to the pool of sedimentary isoGDGTs, thereby influencing the TEX_{86}^{H}. More work is required to assess the effect of the 'deep-water' Thaumarchaeota on the application of TEX_{86}^{H} in the open ocean.

ACKNOWLEDGMENTS

We thank the captain John Ellen and the crew of R/V Pelagia for safe and skillful operation of the ship during the PACEMAKER cruise. Thanks also to Yvo Witte, Ruud Groenewegen, and Marcel Bakker for their invaluable technical support at sea and to Sharyn Ossebaar and Jan van Ooijen for the nutrient analysis at NIOZ. We also acknowledge Henko de Stigter at NIOZ and Silvia Nave at LNEG for their help in the cruise preparation and Henrique Duarte at GeoSurveys for processing the multibeam and seismic data. Stefan Schouten is acknowledged for helpful discussion and Denise Dorhout, Marianne Baas, Jort Ossebaar, Ellen C. Hopmans, and Elda Panoto for their sampling and analytical support at NIOZ. We also acknowledge the four anonymous reviewers who contributed to the improvement of this manuscript with their suggestions. The research leading to these results has received funding from the European Research Council (ERC) under the European Union's Seventh Framework Program (FP7/2007-2013) ERC grant agreement [226600]. This work was carried out under the program of the Netherlands Earth System Science Centre (NESSC).

REFERENCES

Ambar I. and Fiúza A. F. G. (1994) Some features of the Portugal current system: a poleward slope undercurrent, an upwelling related summer southward flow and an autumn–winter poleward coastal surface current. In *Proceedings of the Second International Conference on Air–sea Interaction and on Meteorology and Oceanography of the Coastal Zone* (eds. K. B. Katsaros, A. F. G. Fiúza and I. Ambar). American Meteorological Society, Boston, USA, pp. 286–287.

Baringer M. O. and Pricem J. F. (1997) Mixing and spreading of the Mediterranean outflow. *J. Phys. Oceanogr.* **27**, 1654–1677.

Basse A., Zhu C., Versteegh G. J. M., Fischer G., Hinrichs K.-U. and Mollenhauer G. (2014) Distribution of intact and core tetraether lipids in water column profiles of suspended particulate matter off Cape Blanc, NW Africa. *Org. Geochem.* **72**, 1–13.

Bijl P. K., Bendle J. A., Bohaty S. M., Pross J., Schouten S., Tauxe L., Stickley C. E., McKay R. M., Röhl U., Olney M., Sluijs A., Escutia C., Brinkhuis H. and Expedition 318 Scientists (2013) Eocene cooling linked to early flow across the Tasmanian Gateway. *Proc. Natl. Acad. Sci. U.S.A.* **110**, 9645–9650.

Blumenberg M., Seifert R., Reitner J., Pape T. and Michaelis W. (2004) Membrane lipid patterns typify distinct anaerobic methanotrophic consortia. *Proc. Nat. Acad. Sci. U.S.A.* **101**, 11111–11116.

Brochier-Armanet C., Boussau B., Gribaldo S. and Forterre P. (2008) Mesophilic crenarchaeota: proposal for a third archaeal phylum, the Thaumarchaeota. *Nat. Rev. Microbiol.* **6**, 245–252.

Bryden H. and Stommel H. (1982) Origin of the Mediterranean outflow. *J. Marine Res.* **40**, 55–71.

Candela J. (2001) Mediterranean water and global circulation. In *Ocean Circulation and Climate-Observing and Modelling the Global Ocean, Int. Geophys. Ser.* (eds. G. Siedler, J. Church and J. Gould). Academic Press, San Diego, London, pp. 419–429.

Casey K. and Cornillon P. (1999) A comparison of satellite and in situ-based sea surface temperature climatologies. *J. Climate* **12**, 1848–1863.

Castañeda I. S., Schefuss E., Patzold J., Sinninghe Damsté J. S., Weldeab S. and Schouten S. (2010) Millennial-scale sea surface temperature changes in the eastern Mediterranean (Nile river delta region) over the last 27,000 years. *Paleoceanography* **25**. http://dx.doi.org/10.1029/2009PA001740.

De Jonge C., Stadnitskaia A., Hopmans E. C., Cherkashov G., Fedotov A. and Sinninghe Damsté J. S. (2014) In-situ produced branched glycerol dialkyl glycerol tetraethers in suspended particulate matter from the Yenisei River, Eastern Siberia. *Geochim. Cosmochim. Acta* **125**, 476–491.

DeLong E. F., Preston C. M., Mincer T., Rich V., Hallam S. J. and Frigaard N. U., et al. (2006) Community genomics among stratified microbial assemblages in the ocean's interior. *Science* **311**, 496–503.

Edgar R. C. (2004) MUSCLE: a multiple sequence alignment method with reduced time and space complexity. *BMC Bioinform.* **5**, 113.

Fiúza A. F. G., Macedo M. E. and Guerreiro M. R. (1982) Climatological space and time variation of the Portuguese Coastal Upwelling. *Oceanol. Acta* **5**, 31–40.

Fiúza A. F. G., Hamann M., Ambar I., del Rio G. D., Gonzalez N. and Cabanas J. M. (1998) Water masses and their circulation off western Iberia during May 1993. *Deep Sea Res. I* **45**, 1127–1160.

Francis C. A., Roberts K. J., Beman J. M., Santoro A. E. and Oakley B. B. (2005) Ubiquity and diversity of ammonia-oxidizing archaea in water columns and sediments of the ocean. *Proc. Nat. Acad. Sci. U.S.A.* **102**, 14683–14688.

Harvey H. R., Fallon R. D. and Patton J. S. (1986) The effect of organic-matter and oxygen on the degradation of bacterial-membrane lipids in marine-sediments. *Geochim. Cosmochim. Acta* **50**, 795–804.

Herfort L., Schouten S., Abbas B., Veldhuis M. J. W., Coolen M. J. L., Wuchter C., Boon J. P., Herndl G. J. and Sinninghe Damsté J. S. (2007) Variations in spatial and temporal distribution of Archaea in the North Sea in relation to environmental variables. *FEMS Microbiol. Ecol.* **62**, 242–257.

Hernández-Sánchez M. T., Woodwa E. M. S., Taylor K. W. R., Henderson G. M. and Pancost R. D. (2014) Variations in GDGT distributions through the water column in the South East Atlantic Ocean. *Geochim. Cosmochim. Acta* **132**, 337–348.

Herndl G. J., Reinthaler T., Teira E., van Aken H., Veth C., Pernthaler A. and Pernthaler J. (2005) Contribution of Archaea to total prokaryotic production in the deep Atlantic Ocean. *Appl. Environ. Microbiol.* **71**, 2303–2309.

Hopmans E. C., Weijers J. W. H., Schefuß E., Herfort L., Sinninghe Damsté J. S. and Schouten S. (2004) A novel proxy for terrestrial organic matter in sediments based on branched and isoprenoid tetraether lipids. *Earth Planet. Sci. Lett.* **224**, 107–116.

Hovland M. and Judd A. G. (1988) *Seabed Pockmarks and Seepages: Impact on Geology, Biology and Marine Environment*. Graham and Trotman, London.

Hovland M., Svensen H., Forsberg C. F., Johansen H., Fichler C., Fossa J. H., Jonsson R. and Rueslatten H. (2005) Complex pockmarks with carbonate ridges of mid-Norway: products of sediment degassing. *Mar. Geol.* **218**, 191–206.

Huguet C., Cartes J., Sinninghe Damsté J. S. and Schouten S. (2006) Marine crenarchaeotal membrane lipids in decapods: implications for the TEX_{86} paleothermometer. *Geochem. Geophys. Geosyst.* **7**, Q11010. http://dx.doi.org/10.1029/2006GC001305.

Kaiser J., Ruggieri N., Hefter J., Siegel H., Mollenhauer G., Arz H. W. and Lamy F. (2014) Lipid biomarkers in surface sediments

from the Gulf of Genoa, Ligurian sea (NW Mediterranean sea) and their potential for the reconstruction of palaeo-environments. *Deep-Sea Res. I* **89**, 68–83.

Karner M. B., DeLong E. F. and Karl D. M. (2001) Archaeal dominance in the mesopelagic zone of the Pacific Ocean. *Nature* **409**, 507–510.

Kim J.-H., van der Meer J., Schouten S., Helmke P., Willmott V., Sangiorgi F., Koç N., Hopmans E. C. and Sinninghe Damsté J. S. (2010) New indices and calibrations derived from the distribution of crenarchaeal isoprenoid tetraether lipids: implications for past sea surface temperature reconstructions. *Geochim. Cosmochim. Acta* **74**, 4639–4654.

Kim J.-H., Schouten S., Rodrigo-Gámiz M., Rampen S., Marino G., Huguet C., Helmke P., Buscail R., Hopmans E. C., Pross J., Sangiorgi F., Middelburg J. B. M. and Sinninghe Damsté J. S. (2015) Influence of deep-water derived isoprenoid tetraether lipids on the TEX_{86}^{H} paleothermometer in the Mediterranean Sea. *Geochim. Cosmochim. Acta* **150**, 125–141.

Kinder T. H. and Parrilla G. (1987) Yes, some of the mediterranean outflow does come from great depth. *J. Geophys. Res. Oceans* **92**, 2901–2906.

Könneke M., Bernhard A. E., de la Torre J., Walker C. B., Waterbury J. B. and Stahl D. A. (2005) Isolation of an autotrophic ammonia-oxidizing marine archaeon. *Nature* **437**, 543–546.

Lengger S. K., Hopmans E. C., Sinninghe Damsté J. S. and Schouten S. (2012) Comparison of extraction and work up techniques for analysis of core and intact polar tetraether lipids from sedimentary environments. *Org. Geochem.* **47**, 34–40.

Lincoln S. A., Wai B., Eppley J. M., Church M. J., Summons R. E. and DeLong E. F. (2014a) Planktonic Euryarchaeota are a significant source of archaeal tetraether lipids in the ocean. *Proc. Natl. Acad. Sci. U.S.A.* **111**, 9858–9863.

Lincoln S. A., Wai B., Eppley J. M., Church M. J., Summons R. E. and DeLong E. F. (2014b) Reply to Schouten et al.: Marine Group II planktonic Euryarchaeota are significant contributors to tetraether lipids in the ocean. *Proc. Natl. Acad. Sci. U.S.A.* **111**, E4286.

Littler K., Robinson S. A., Bown P. R., Nederbragt A. J. and Pancost R. D. (2011) High sea-surface temperatures during the Early Cretaceous Epoch. *Nat. Geosci.* **4**, 169–172.

Locarnini R. A., Mishonov A. V., Antonov J. I., Boyer T. P., Garcia H. E., Baranova O. K., Zweng M. M., Paver C. R., Reagan J. R., Johnson D. R., Hamilton M. and Seidov D. (2013) World Ocean Atlas 2013, Volume 1: Temperature. In *A. Mishonov Technical Ed.* (ed. S. Levitus). NOAA Atlas NESDIS 73, 40 p.

Logemann J., Graue J., Köster J., Engelen B., Rullkötter J. and Cypionka H. (2011) A laboratory experiment of intact polar lipid degradation in sandy sediments. *Biogeosciences* **8**, 2547–2560.

Ludwig W., Strunk O., Westram R., Richter L., Meier H., Yadhukumar Buchner A., Lai T., Steppi S., Jobb G., Förster W., Brettske I., Gerber S., Ginhart A. W., Gross O., Grumann S., Hermann S., Jost R., König A., Liss T., Lüßmann R., May M., Nonhoff B., Reichel B., Strehlow R., Stamatakis A., Stuckmann N., Vilbig A., Lenke M., Ludwig T., Bode A. and Schleifer K.-H. (2004) ARB: a software environment for sequence data. *Nucl. Acids Res.* **32**, 1363–1371.

Martins C. S., Hamann M. and Fuiza A. F. G. (2002) Surface circulation in the eastern North Atlantic from drifters and altimetry. *J. Geophys. Res.* **107**, 3217. http://dx.doi.org/10.1029/2000JC000345.

Pancost R. D., Hopmans E. C., Sinninghe Damsté J. S. and Party Medinauth Scientific. (2001) Archaeal lipids in Mediterranean cold seeps: molecular proxies for anaerobic methane oxidation. *Geochim. Cosmochim. Acta* **65**, 1611–1627.

Pearson A., McNichol A. P., Benitez-Nelson B. C., Hayes J. M. and Eglinton T. I. (2001) Origins of lipid biomarkers in Santa Monica Basin surface sediment: a case study using compound-specific $\Delta^{14}C$ analysis. *Geochim. Cosmochim. Acta* **65**, 3123–3137.

Pester M., Rattei T., Flechl S., Gröngröft A., Richter A., Overmann J., Reinhold-Hurek B., Loy A. and Wagner M. (2012) *amo*A-based consensus phylogeny of ammonia-oxidizing archaea and deep sequencing of *amo*A genes in soils of four different geographic regions. *Environ. Microbiol.* **14**, 525–539.

Pitcher A., Hopmans E. C., Schouten S. and Sinninghe Damsté J. S. (2009) Separation of core and intact polar archaeal tetraether lipids using silica columns: insights into living and fossil biomass contributions. *Org. Geochem.* **40**, 12–19.

Pitcher A., Villanueva L., Hopmans E. C., Schouten S., Reichart G. J. and Sinninghe Damsté J. S. (2011) Niche segregation of ammonia-oxidizing archaea and anammox bacteria in the Arabian Sea oxygen minimum zone. *ISME J.* **5**, 1896–1904.

Puig P., Durrieu de Madron X., Salat J., Schroeder K., Martín J., Karageorgis A. P., Palanques A., Roullier F., Lopez-Jurado J. L., Emelianov M., Moutin T. and Houpert L. (2013) Thick bottom nepheloid layers in the western Mediterranean generated by deep dense shelf water cascading. *Prog. Oceanogr.* **111**, 1–23.

Qin W., Amin S. A., Martens-Habbena W., Walker C. B., Urakawa H., Devol A. H., Ingalls A. E., Moffett J. W., Armbrust E. V. and Stahl D. A. (2014) Marine ammonia-oxidizing archaeal isolates display obligate mixotrophy and wide ecotypic variation. *Proc. Natl. Acad. Sci. U.S.A.* **111**, 12504–12509.

Quaresma L. S., Vitorino J., Oliveira A. and da Silva J. (2007) Evidence of sediment resuspension by nonlinear internal waves on the western Portuguese mid-shelf. *Mar. Geol.* **246**, 123–143.

Saitou N. and Nei M. (1987) The neighbor-joining method: a new method for reconstructing phylogenetic trees. *Mol. Biol. Evol.* **4**, 406–425.

Sánchez-Goñi M. F. and Harrison S. P. (2010) Millennial-scale climate variability and vegetation changes during the last glacial: concepts and terminology. *Quat. Sci. Rev.* **29**, 2823–2827.

Santoro A. E., Casciotti K. L. and Francis C. A. (2010) Activity, abundance and diversity of nitrifying archaea and bacteria in the central California Current. *Environ. Microbiol.* **12**, 1989–2006.

Saunders P. M. (1982) Circulation in the eastern North Atlantic. *J. Mar. Res.* **40**, 641–657.

Schouten S., Hopmans E. C., Pancost R. D. and Sinninghe Damsté J. S. (2000) Widespread occurrence of structurally diverse tetraether membrane lipids: evidence for the ubiquitous presence of low-temperature relatives of hyperthermophiles. *Proc. Natl. Acad. Sci. U.S.A.* **97**, 14421–14426.

Schouten S., Hopmans E. C., Schefuß E. and Sinninghe Damsté J. S. (2002) Distributional variations in marine crenarchaeotal membrane lipids: a new tool for reconstructing ancient sea water temperatures? *Earth Planet. Sci. Lett.* **204**, 265–274.

Schouten S., Hopmans E. C., Forster A., van Breugel Y., Kuypers M. M. M. and Sinninghe Damsté J. S. (2003) Extremely high sea-surface temperatures at low latitudes during the middle Cretaceous as revealed by archaeal membrane lipids. *Geology* **31**, 1069–1072.

Schouten S., Huguet C., Hopmans E. C., Kienhuis M. and Sinninghe Damsté J. S. (2007) Analytical methodology for TEX_{86} paleothermometry by high-performance liquid chro-

matography/atmospheric pressure chemical ionization-mass spectrometry. *Anal. Chem.* **79**, 2940–2944.

Schouten S., Pitcher A., Hopmans E. C., Villanueva L., van Bleijswijk J. and Sinninghe Damsté J. S. (2012) Intact polar and core glycerol dibiphytanyl glycerol tetraether lipids in the Arabian Sea oxygen minimum zone: I. Selective preservation and degradation in the water column and consequences for the TEX_{86}. *Geochim. Cosmochim. Acta* **98**, 228–243.

Schouten S., Hopmans E. C. and Sinninghe Damsté J. S. (2013) The organic geochemistry of glycerol dialkyl glycerol tetraether lipids: a review. *Org. Geochem.* **54**, 19–61.

Schouten S., Villanueva L., Hopmans E. C., van der Meer M. T. and Sinninghe Damsté J. S. (2014) Are Marine Group II Euryarchaeota significant contributors to tetraether lipids in the ocean? *Proc. Natl. Acad. Sci. U.S.A.* **111**, E4285.

Shackleton N. J., Hall M. A. and Vincent E. (2000) Phase relationships between millennial-scale events 64,000–24,000 years ago. *Paleoceanography* **15**, 565–569.

Shah S. R., Mollenhauer G., Ohkouchi N., Eglinton T. I. and Pearson A. (2008) Origins of archaeal tetraether lipids in sediments: insights from radiocarbon analysis. *Geochim. Cosmochim. Acta* **72**, 4577–4594.

Sinninghe Damsté J. S., Hopmans E. C., Schouten S., van Duin A. C. T. and Geenevasen J. A. J. (2002) Crenarchaeol: The characteristic core glycerol dibiphytanyl glycerol tetraether membrane lipid of cosmopolitan pelagic crenarchaeota. *J. Lipid Res.* **43**, 1641–1651.

Smittenberg R. H., Hopmans E. C., Schouten S., Hayes J. M., Eglinton T. I. and Sinninghe Damsté J. S. (2004) Compound-specific radiocarbon dating of the varved Holocene sedimentary record of Saanich Inlet, Canada. *Paleoceanography* **19** (PA2012), 2003PA000927.

Spang A., Hatzenpichler R., Brochier-Armanet C., Rattei T., Tischler P., Spieck E., Streit W., Stahl D. A., Wagner M. and Schleper C. (2010) Distinct gene set in two different lineages of ammoniaoxidizing archaea supports the phylum Thaumarchaeota. *Trends Microbiol.* **18**, 331–340.

Taylor K. W. R., Huber M., Hollis C. J., Hernandez-Sanchez M. T. and Pancost R. D. (2013) Re-evaluating modern and Paleogene GDGT distributions: implications for SST reconstructions. *Global Planet. Change* **108**, 158–174.

Turich C., Schouten S., Thunell R. C., Varela R., Astor Y. and Wakeham S. G. (2013) Comparison of TEX86 and $U^{K'}_{37}$ temperature proxies in sinking particles in the Cariaco Basin. *Deep-Sea Res. I* **78**, 115–133.

van Aken H. M. (2000) The hydrography of the mid-latitude Northeast Atlantic Ocean II: the intermediate water masses. *Deep-Sea Res. I* **47**, 789–824.

van Haren H. and Millot C. (2004) Rectilinear and circular inertial motions in the Western Mediterranean Sea. *Deep-Sea Res. I* **51**, 1441–1455.

Vanney J. R. and Mougenot D. (1981) La plate-forme continentale de Portugal et Ics provinces adjacentes: analyse geomorphologique. *Memb. Serv. Geol. Port.* **28**, 1–86.

Villanueva L., Schouten S. and Sinninghe Damsté J. S. (2014) A re-evaluation of the archaeal membrane lipid biosynthetic pathway. *Nat. Rev. Microbiol.* **12**, 438–448.

Villanueva L., Schouten S. and Sinninghe Damsté J. S. (2015) Depth-related distribution of a key gene of the tetraether lipid biosynthetic pathway in marine Thaumarchaeota. *Environ. Microbiol.*. http://dx.doi.org/10.1111/1462-2920.12508.

Voelker A. H. L. and de Abreu L. (2011) A review of abrupt climate change events in the Northeastern Atlantic Ocean (Iberian margin): latitudinal, longitudinal, and vertical gradients. In *Abrupt climate change: mechanisms, patterns, and impacts* (eds. H. Rashid, L. Polyak, E. Mosley-Thompson). American Geophysical Union, Washington, DC., Geophys. Monogr. Ser. 193, pp. 15–37.

Wakeham S. G., Lewis C. M., Hopmans E. C., Schouten S. and Sinninghe Damsté J. S. (2003) Archaea mediate anaerobic oxidation of methane in deep euxinic waters of the Black Sea. *Geochim. Cosmochim. Acta* **67**, 1359–1374.

Weijers J. W. H., Schouten S., Spaargaren O. C. and Sinninghe Damsté J. S. (2006) Occurrence and distribution of tetraether membrane lipids in soils: implications for the use of the TEX_{86} proxy and the BIT index. *Org. Geochem.* **37**, 1680–1693.

Weijers J. W. H., Bernhardt B., Peterse F., Werne J. P., Dungait J. A. J., Schouten S. and Sinninghe Damsté J. S. (2011a) Absence of seasonal patterns in MBT-CBT indices in mid-latitude soils. *Geochim. Cosmochim. Acta* **75**, 3179–3190.

Weijers J. W. H., Lim K., Aquilina A., Sinninghe Damsté J. S. and Pancost R. D. (2011b) Biogeochemical controls on glycerol dialkyl glycerol tetraether lipid distributions in sediments characterized by diffusive methane flux. *Geochem. Geophys. Geosyst.* **12**, Q10010. http://dx.doi.org/10.1029/2011GC003724.

Wuchter C., Schouten S., Wakeham S. G. and Sinninghe Damsté J. S. (2005) Temporal and spatial variation in tetraether membrane lipids of marine Crenarchaeota in particulate organic matter: implications for TEX_{86} paleothermometry. *Paleoceanography* **20**, 1–11.

Xie S., Lipp J. S., Wegener G., Ferdelman T. G. and Hinrichs K.-U. (2013) Turnover of microbial lipids in the deep biosphere and growth of benthic archaeal populations. *Proc. Natl. Acad. Sci. U.S.A.* **110**, 6010–6014.

Yakimov M. M., Cono V. L., Smedile F., DeLuca T. H., Juarez S., Ciordia S., Fernández M., Albar J. P., Ferrer M., Golyshin P. N. and Giuliano L. (2011) Contribution of crenarchaeal autotrophic ammonia oxidizers to the dark primary production in Tyrrhenian deep waters (Central Mediterranean Sea). *ISME J.* **5**, 945–961.

Zell C., Kim J.-H., Abril G., Sobrinho R. L., Dorhout D., Moreira-Turcq P. and Sinninghe Damsté J. S. (2013a) Impact of seasonal hydrological variation on the distributions of tetraether lipids along the Amazon River in the central Amazon basin: implications for the MBT/CBT paleothermometer and the BIT index. *Front. Microbiol.* **4**. http://dx.doi.org/10.3389/fmicb.2013.00228.

Zell C., Kim J.-H., Moreira-Turcq P., Abril G., Hopmans E. C., Bonnet M.-P., Sobrinho R. L. and Sinninghe Damsté J. S. (2013b) Disentangling the origins of branched tetraether lipids and crenarchaeol in the lower Amazon River: implications for GDGT-based proxies. *Limnol. Ocean.* **58**, 343–353.

Zell C., Kim J.-H., Balsinha M., Dorhout D., Fernandes C., Baas M. and Sinninghe Damsté J. S. (2014) Transport of branched tetraether lipids from the Tagus River basin to the coastal ocean of the Portuguese margin: consequences for the interpretation of the MBT'/CBT paleothermometer. *Biogeosciences* **11**, 5637–5655.

Zell C., Kim J.-H., Dorhout D., Baas M. and Sinninghe Damsté J. S. (2015) Sources and distributions of branched tetraether lipids and crenarchaeol along the Portuguese continental margin. *Cont. Shelf Res.* **96**, 34–44.

Zweng M. M, Reagan J. R., Antonov J. I., Locarnini R. A., Mishonov A. V., Boyer T. P., Garcia H. E., Baranova O. K., Johnson D. R., Seidov D. and Biddle M. M. (2013) World Ocean Atlas 2013, Volume 2: Salinity. In A. *Mishonov Technical Ed.* (ed. S. Levitus). NOAA Atlas NESDIS 74, 39 pp.

Associate editor: Thomas Wagner